Steady-state solutions in mathematical models of atrial cell electrophysiology and their stability

Vincent Jacquemet[a]

[a]*Signal Processing Institute, Ecole Polytechnique Fédérale de Lausanne (EPFL)*
CH–1015 Lausanne, Switzerland
vincent.jacquemet@umontreal.ca

Published in:

Math. Biosci. (2007), vol. 208, pp. 241-269.

Abstract

The steady states of the Fenton-Karma, the Courtemanche and the Nygren cell models were studied by determining the fixed points of the dynamical system describing their cell kinetics. The linear stability of the fixed points was investigated, as well as their response to external stimuli. Symbolic calculations were carried out as far as possible in order to prove the existence of these fixed points. In the Fenton–Karma model, a unique stable fixed point was found, namely the resting state. In contrast, the Courtemanche model had an infinite number of fixed points. A bifurcation diagram was constructed by classifying these fixed points according to a conservation law. Initial conditions were identified, for which the dynamical behavior of the cell was auto-oscillatory. In its original formulation, the Nygren model had no fixed point. After having restored charge conservation, the system was found to have an infinite number of fixed points, resulting in a bifurcation diagram similar to that of the Courtemanche model. The approach proposed in this paper assists in the exploration of the high-dimensional parameter space of the cell models and the identification of the conditions leading to spontaneous pacemaker activity.

Keywords: cardiac electrophysiology; cardiac cell model; resting potential; steady state; ionic concentration.

1. Introduction

Different mathematical models have been formulated to describe cardiac cell electrophysiology [1]. In these models, the evolution of the state of the cell (transmembrane potential, ionic concentrations, etc.) is governed by a set of coupled non-linear differential equations. In the framework of dynamical system theory, it is natural to start the analysis of such systems by identifying the fixed points, that is, the steady-state solutions to the equations. If these fixed points are stable, they correspond to resting states, whereas unstable fixed points may potentially induce pacemaker activity. This identification is complicated if the number of equations involved is high (more than 20–30 in the recent models) and by the complexity of the mathematical formulation. In this paper, analytical methods are applied to determine the comprehensive set of fixed points of two recent human atrial cell models, the Courtemanche model [2] and the Nygren [3] model.

The motivation for this work reflects the multidisciplinary nature of mathematical modeling. First, from the physical viewpoint, we would expect the resting state to be unique and stable in mathematical models. Although real non-pacemaker cardiac myocytes may not be able to maintain ionic homeostasis over a long period, the stability of the resting potential is often postulated in theoretical studies [4, 5]. It is therefore desirable to demonstrate mathematically the consistency of the models with respect to this empirical expectation. The so-called second generation ventricular cell models that take into account variations in ionic concentrations were found to have an infinite number of steady states [6–8]. We will see that this is also the case for the Courtemanche model, but no resting state exists for the Nygren model in its original formulation. A complete and accurate description of the fixed points of the models provides additional information for comparing the existing models in their ability to reproduce the basic properties of real cells.

Next, from the computer simulation viewpoint, the resting state is often used as initial condition for the simulations. The resting state is generally computed by letting the system evolve from an arbitrary initial state until the steady state is reached. This method implicitly

assumes that the resting state is unique and stable, which is restrictive if no fixed point is stable, like for pacemaker cells. More generally, it is physiologically questionable to assume that cardiac cells are able to indefinitely maintain a stable equilibrium when left unstimulated. Also, slow transient drifts in ionic concentrations make it difficult to establish that the steady state is indeed reached [8, 9]. These limitations do not affect the method presented in this paper.

Furthermore, from the biophysical modeling viewpoint, the parameters of the cardiac cell models often need to be significantly modified in order to reproduce spatial heterogeneity and pathological or patient-specific properties [10–12]. The resting state can be affected by this operation. Reciprocally, we sometimes aim at altering the resting potential to incorporate in computer models its spatial variations, like those reported in the sleeves of the pulmonary vein [13]. This inverse procedure is facilitated if a fast and reliable method for computing the resting state is available.

Finally, from the mathematical viewpoint, the formulation of each ion channel can have an impact on the global properties of the cell model (such as the number of fixed points). For example, Varghese and Sell showed the importance of the formulation of the Na^+/Ca^{2+} exchanger to avoid a possible divergence in finite time [14]. Here, we will see how a slightly different mathematical expression for the inward rectifier potassium current I_{K1} can create additional fixed points.

In this paper, the generic formulation of the cardiac cell model is first introduced. After presenting the methodology, it is illustrated by its application to the relatively simple Fenton–Karma model. The steady-state solutions of the Courtemanche and the Nygren models are then exhibited and interpreted. The existence of a conservation law plays a central role in this derivation. Special attention is devoted to ensure that this condition is indeed satisfied. The differences between the models are discussed. The equations of the Courtemanche and Nygren models are recalled in the Appendices Appendix A and Appendix B in order to define the unified notations used in this paper. The reader is referred to the original articles

[2, 3] for the complete details.

2. Methodology

2.1. Generic formulation

The dynamics of cardiac cell electrophysiology is described by a set of ordinary differential equations

$$\frac{\mathrm{d}\mathbf{x}}{\mathrm{d}t} = \mathbf{f}(\mathbf{x}) \quad . \tag{1}$$

The state $\mathbf{x}$ of the cell is typically written as

$$\mathbf{x} = (V, \mathbf{c}, \mathbf{y}) \quad , \tag{2}$$

where V is the transmembrane potential (the intracellular potential minus the extracellular potential), $\mathbf{y}$ represents the set of gating variables and $\mathbf{c}$ the ionic concentration of the different ions present in the intra- or extracellular space, or in internal cell compartments. The transmembrane potential satisfies the equation

$$C_m \frac{\mathrm{d}V}{\mathrm{d}t} = -I_{\mathrm{ion}}(\mathbf{x}) \quad , \tag{3}$$

where C_m is the cell membrane capacitance and I_{ion} is the outward-oriented membrane current. The component of Eq. (1) corresponding to the i-th gating variable is an equation of the type

$$\frac{\mathrm{d}y_i}{\mathrm{d}t} = \frac{y_{i_\infty}(\mathbf{x}) - y_i}{\tau_{y_i}(\mathbf{x})} \quad . \tag{4}$$

The steady-state value y_{i_∞} always lies between 0 and 1. The variable τ_{y_i} is the relaxation time, which is positive. As a result, $0 \leq y_i(t) \leq 1$, provided that $0 \leq y_i(t=0) \leq 1$. The evolution of the ionic concentrations is expressed using the ionic flux Φ

$$\frac{\mathrm{d}\mathbf{c}}{\mathrm{d}t} = \Phi(\mathbf{x}) \quad . \tag{5}$$

2.2. Steady-state solutions

A steady state is any fixed point of Eq. (1), that is, a solution $\overline{\mathbf{x}}$ to the equation

$$\mathbf{f}(\mathbf{x}) = 0 \quad . \tag{6}$$

For any function of the state variables $X(\mathbf{x})$, its steady-state value is denoted by $\overline{X} = X(\overline{\mathbf{x}})$. In general, the dynamics of a gating variable is not affected by the other gating variables. This implies that Eq. (6) is solved easily for the gating variables:

$$\overline{y_i} = y_{i_\infty}\left(\overline{V}, \overline{\mathbf{c}}\right) \quad . \tag{7}$$

These values can be substituted in Eq. (6) and lead to the following system:

$$I_{\text{ion}}\left(\overline{\mathbf{y}}\left(\overline{V}, \overline{\mathbf{c}}\right), \overline{V}, \overline{\mathbf{c}}\right) = 0 \tag{8}$$

$$\Phi\left(\overline{\mathbf{y}}\left(\overline{V}, \overline{\mathbf{c}}\right), \overline{V}, \overline{\mathbf{c}}\right) = 0 \quad . \tag{9}$$

For solving this system, an analytical approach is to be preferred when computing the comprehensive list of fixed points in order to avoid root-finding in a high dimensional space. For the cell models considered in this paper, this system will be reduced to a set of single-variable equations for which the number of roots can be worked out.

2.3. Conservation law

Suppose that a conservation law exists for the system, *i.e.*, a function $Q(V, \mathbf{c})$ such that $\mathrm{d}Q/\mathrm{d}t = 0$. In this case, $Q(V, \mathbf{c}) = Q_0$, where Q_0 is computed from the initial condition. Then, V becomes a function of $\mathbf{c}$, that is, $V = \mathcal{V}(\mathbf{c}; Q_0)$. For each possible value of Q_0, Eq. (9) reduces to an equation for $\overline{\mathbf{c}}$ only

$$\Phi\Big(\overline{\mathbf{y}}\left(\mathcal{V}(\overline{\mathbf{c}}; Q_0), \overline{\mathbf{c}}\right), \mathcal{V}(\overline{\mathbf{c}}; Q_0), \overline{\mathbf{c}}\Big) = 0 \quad , \tag{10}$$

and Eq. (8) is only used to check the consistency of the solution. Therefore, as a result of the existence of a conservation law, continuous sets of fixed points indexed by Q_0 may be found.

2.4. Response to small perturbations

The response to small perturbation is analyzed by linearizing the system around the fixed point. In particular, the stability of a fixed point $\overline{\mathbf{x}}$ is established by computing the eigenvalues of the Jacobian matrix $D\mathbf{f}(\overline{\mathbf{x}})$. If the real part of all the eigenvalues of $D\mathbf{f}$ is negative, then the fixed point is stable. Although $D\mathbf{f}$ could have been computed analytically (for example by means of a computer algebra system), the Jacobian matrix of the detailed cell models studied in this paper was estimated using the centered finite difference approximation:

$$D\mathbf{f}(\overline{\mathbf{x}})_{i,j} = \frac{\partial f_i}{\partial x_j}(\overline{\mathbf{x}}) = \frac{f_i(\overline{\mathbf{x}} + h_j \mathbf{e}_j) - f_i(\overline{\mathbf{x}} - h_j \mathbf{e}_j)}{2h_j} + \mathcal{O}(h_j) \quad , \tag{11}$$

where $\mathbf{e}_j = (0, \ldots, 0, 1, 0, \ldots)$ with a "1" at the j-th position. The eigenvalues were computed using MATLAB (Mathworks Inc., Natick, MA, USA).

2.5. Response to large perturbations

When a fixed point is stable, a small perturbation gives rise to a linear response. A larger perturbation may initiate an action potential [1]. In order to study these non-linear responses, Eq. (3) is replaced by

$$C_m \frac{\mathrm{d}V}{\mathrm{d}t} = -I_{\mathrm{ion}}(\mathbf{x}) + I_{\mathrm{stim}}(t) \quad , \tag{12}$$

where $I_{\mathrm{stim}}(t)$ is an external driving force (stimulation current), typically a train of square pulses. In order to computed action potentials, the differential equations [Eqs. (4), (5) and (12)] were solved numerically using the forward Euler method, with a time step of 10 μs.

2.6. Example: the Fenton–Karma model

The methodology presented above is applied in this subsection to the Fenton–Karma model [15]. This simplified cardiac cell model was developed to reproduce the experimentally observed rate dependence of action potential duration and conduction velocity, while keeping the computational complexity as low as possible. The model is based on three variables: the

(dimensionless) transmembrane potential u, and two gating variables v and w. The evolution of these state variables is governed by the following set of equations [15]:

$$\frac{\mathrm{d}u}{\mathrm{d}t} = -I_{\mathrm{fi}} - I_{\mathrm{so}} - I_{\mathrm{si}} \tag{13}$$

$$\frac{\mathrm{d}v}{\mathrm{d}t} = \Theta(u_c - u)\,\frac{1-v}{\tau_v^-(u)} - \Theta(u-u_c)\,\frac{v}{\tau_v^+} \tag{14}$$

$$\frac{\mathrm{d}w}{\mathrm{d}t} = \Theta(u_c - u)\,\frac{1-w}{\tau_w^-} - \Theta(u-u_c)\,\frac{w}{\tau_w^+} \tag{15}$$

$$I_{\mathrm{fi}} = -\frac{v}{\tau_{\mathrm{d}}}\Theta(u-u_c)\,(1-u)(u-u_c) \tag{16}$$

$$I_{\mathrm{so}} = \frac{u}{\tau_0}\,\Theta(u_c-u) + \frac{1}{\tau_{\mathrm{r}}}\,\Theta(u-u_c) \tag{17}$$

$$I_{\mathrm{si}} = -\frac{w}{2\tau_{\mathrm{si}}}\,\left(1+\tanh\left(k\left(u-u_c^{\mathrm{si}}\right)\right)\right) \tag{18}$$

$$\tau_v^-(u) = \Theta(u-u_v)\,\tau_{v,1}^- + \Theta(u_v-u)\,\tau_{v,2}^- \tag{19}$$

where $\Theta(x) = 1$ if $x \geq 0$ and 0 otherwise. This model depends on 13 parameters u_c, u_v, u_c^{si}, k, τ_{si}, $\tau_{v,1}^-$, $\tau_{v,2}^-$, τ_v^+, τ_w^-, τ_w^+, τ_{d}, τ_0, τ_{r}, all of which are positive. No conservation law exists for this model.

The steady state is found by setting the time derivatives to zero in Eqs. (13)–(15). First, assume that $\overline{u} > u_c$. Then, $\overline{v} = \overline{w} = 0$ so that Eq. (13) implies $1/\tau_{\mathrm{r}} = 0$, which is impossible. Therefore, we will look for values of $\overline{u}$ such that $\overline{u} < u_c$. In this case, $\overline{v} = \overline{w} = 1$ and $\overline{u}$ is a root of the equation

$$\frac{2\tau_{\mathrm{si}}}{\tau_0}\,\overline{u} = 1 + \tanh\left(k\left(\overline{u} - u_c^{\mathrm{si}}\right)\right) \quad . \tag{20}$$

This equation has one, two or three positive solutions, depending on the value of the parameters. Since $\tanh x$ is convex for $x \leq 0$, the condition $\tau_{\mathrm{si}} u_c^{\mathrm{si}} > \tau_0$ ensures the uniqueness of the solution. This condition is satisfied for all sets of parameters fitted to atrial [12] and ventricular [15] electrophysiological cell properties. Since $\overline{u} < u_c$ and $u_c \ll u_c^{\mathrm{si}}$ for all of these parameter sets, an approximation for $\overline{u}$ is found by noting that $\frac{1}{2}(1+\tanh x) \approx \exp(2x)$ asymptotically for $x \to -\infty$. After some algebraic manipulations, we obtain

$$0 \;<\; \overline{u} \;\approx\; -\frac{1}{2k}\,W\left(-\frac{2k\tau_0}{\tau_{\mathrm{si}}}\,\exp\left(-2ku_c^{\mathrm{si}}\right)\right) \;\approx\; \frac{\tau_0}{\tau_{\mathrm{si}}}\,\exp\left(-2ku_c^{\mathrm{si}}\right) \quad , \tag{21}$$

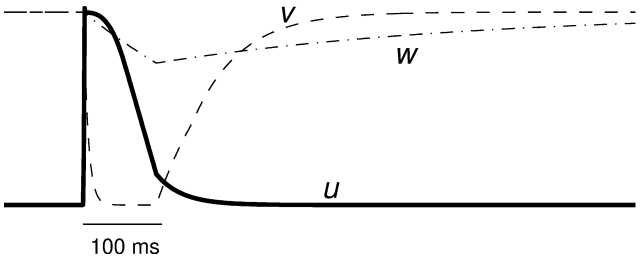

Figure 1: Time course of the variables u, v and w of the atrial variant of the Fenton–Karma model. The range of the vertical axis is 1 because the variables are dimensionless.

where W is the Lambert's W function [16], defined for arguments $\geq -1/e$ as the inverse of the function $x\ \exp(x)$. The second approximation in Eq. (21) results from the Taylor expansion $W(x) = x + \mathcal{O}(x^2)$.

Establishing the stability of the steady-state is facilitated by the fact the involved Jacobian matrix is upper triangular. Its diagonal entries are:

$$-\frac{1}{\tau_0} + \frac{k}{2\tau_{\mathrm{si}}}\Big(1 - \tanh^2\left(k\left(\overline{u} - u_c^{\mathrm{si}}\right)\right)\Big)\ , \qquad -\frac{1}{\tau_v^-(\overline{u})} \qquad \text{and} \qquad -\frac{1}{\tau_w^-}\ . \tag{22}$$

A sufficient condition for ensuring the stability of the steady state is therefore

$$1 - \tanh^2\big(k\left(u_c - u_c^{\mathrm{si}}\right)\big) < \frac{2\tau_{\mathrm{si}}}{k\tau_0}\ , \tag{23}$$

since $\overline{u} < u_c$. This condition is satisfied for the various parameter sets of the Fenton–Karma model [12, 15].

An action potential was simulated in the Fenton–Karma model with the parameter set corresponding to atrial cells remodeled during chronic atrial fibrillation [12]. The steady-state $\overline{u} = 1.18 \cdot 10^{-8}$ and $\overline{v} = \overline{w} = 1$ was used as initial condition. A stimulus of strength 0.2 and duration 2 ms was applied at time $t = 100$ ms. The time course of the variables is shown on Fig. 1. After the repolarization phase the action potential, the variables can be seen to return to their steady-state value.

In conclusion, the Fenton–Karma model can be easily proved to have a unique and stable

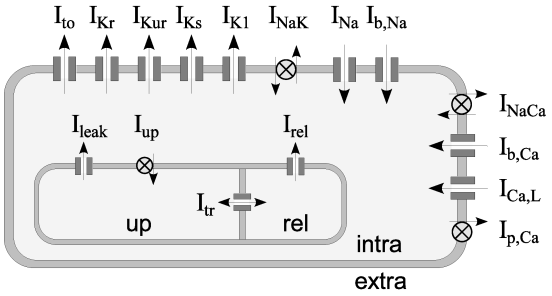

Figure 2: Schematic view of the Courtemanche model, illustrating its membrane currents, pumps and ion exchangers. The different compartments are indicated: the extracellular (extra) and intracellular (intra) media, and, in the sarcoplasmic reticulum, the uptake (up) and release (rel) compartment.

steady-state, the resting state, in agreement with our expectations. More complex models can be treated by the same methodology, as demonstrated in the sequel.

3. Conservation law in atrial cell models

In this section, the Courtemanche and the Nygren models are briefly introduced, with special emphasis on the derivation of a conservation law. The notations as well as the mathematical formulation of the models are recapitulated in Appendices Appendix A and Appendix B, cast in a unified notation.

3.1. The Courtemanche model

The Courtemanche model [2] comprises 21 state variables in total: the transmembrane potential V; 5 ionic concentrations: $[Na^+]_i$, $[K^+]_i$, $[Ca^{++}]_i$, $[Ca^{++}]_{up}$ and $[Ca^{++}]_{rel}$ in 3 fluid compartments: the intracellular compartment (index "i"), and the uptake and release compartments of the sarcoplasmic reticulum (indices "up" and "rel" respectively); and 15 gating variables: m, h, j, o_a, o_i, u_a, u_i, x_r, x_s, d, f, f_{Ca}, u, v and w. The ionic currents flowing between the different compartments are illustrated on Fig. 2. The evolution equations are listed in Appendix Appendix A.

These 21 state variables are not independent, because a charge conservation law is involved, which relates these variables. This conservation principle is associated with ionic charge balance, as was previously reported for the DiFrancesco–Noble [6, 14] and the Luo–Rudy dynamic model [8]. It formed the basis for the construction of the Endresen model [17]. Here, the approach sketched in subsection 2.3 is applied to the Courtemanche model.

The cell membrane acts as a capacitor, which means that $C_m V = Q_i$ where Q_i is the electric charge in the inner side of the capacitor, that is, within the cell [1]. The charge Q_i is the sum of the charges carried by the Na^+, K^+ and Ca^{2+} ions, as well as by other ions, notably anions. This last term will be called the non-specific charge $-Q_{\rm ns}$. The charge carried by a specific ion within a compartment can be computed as its valence $\times$ its concentration $\times$ the volume of the compartment $\times$ the Faraday constant F. The equation of a capacitor therefore reads

$$C_m V = V_{\rm i} F \Big([{\rm Na^+}]_{\rm i} + [{\rm K^+}]_{\rm i} + 2\,[{\rm Ca^{++}}]_{\rm i} + 2\,[{\rm Ca^{++}}]_{\rm Trpn} + 2\,[{\rm Ca^{++}}]_{\rm Cmdn} \Big) + 2\,V_{\rm up} F\,[{\rm Ca^{++}}]_{\rm up} + 2\,V_{\rm rel} F \Big([{\rm Ca^{++}}]_{\rm rel} + [{\rm Ca^{++}}]_{\rm Csqn} \Big) - Q_{\rm ns} \quad . \tag{24}$$

This equation expresses the dependence between the transmembrane potential and the ionic concentrations and is considered to be the *definition* of $Q_{\rm ns}$ for the Courtemanche model. The time derivative of $Q_{\rm ns}$ is derived from Eqs. (A.11)–(A.16) and (A.19)–(A.20), from which it is established that

$$\frac{{\rm d}Q_{\rm ns}}{{\rm d}t} = 0 \quad . \tag{25}$$

Hence, the charge $Q_{\rm ns}$ is conserved. It is positive when the resting potential is negative. It is convenient to write this constant charge as

$$Q_{\rm ns} = V_{\rm i} F\,[{\rm NS}]_{\rm i} \quad , \tag{26}$$

where the non-specific charge concentration $[{\rm NS}]_{\rm i}$ is expressed in mM. Typical relevant values of $[{\rm NS}]_{\rm i}$ are chosen such that the net charge difference between intra- and extracellular media

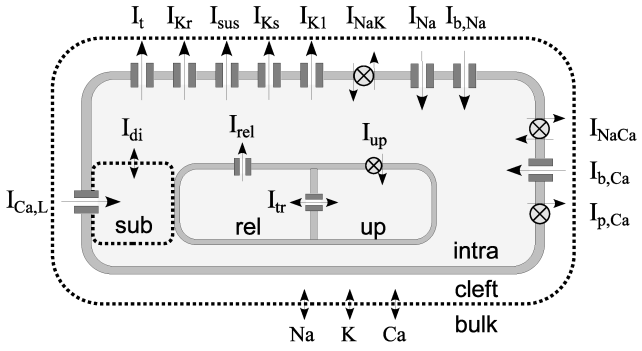

Figure 3: Schematic view of the Nygren model, illustrating its membrane currents, pumps and ion exchangers. The different compartments are indicated: the extracellular (bulk), cleft, and intracellular (intra) media, the subsarcolemal domain (sub), and, in the sarcoplasmic reticulum, the uptake (up) and release (rel) compartment.

is close to zero at zero membrane potential [17]. Alternatively, $[\mathrm{NS}]_\mathrm{i}$ can be computed by substituting in Eq. (24) the initial values for the ionic concentrations [8].

3.2. The Nygren model

The Nygren model comprises 29 state variables in total: the transmembrane potential V; 9 ionic concentrations: $[\mathrm{Na}^+]_\mathrm{c}$, $[\mathrm{K}^+]_\mathrm{c}$, $[\mathrm{Ca}^{++}]_\mathrm{c}$, $[\mathrm{Na}^+]_\mathrm{i}$, $[\mathrm{K}^+]_\mathrm{i}$, $[\mathrm{Ca}^{++}]_\mathrm{i}$, $[\mathrm{Ca}^{++}]_\mathrm{d}$, $[\mathrm{Ca}^{++}]_\mathrm{up}$ and $[\mathrm{Ca}^{++}]_\mathrm{rel}$ in 5 fluid compartments: the cleft compartment (in the extracellular space, index "c"), the intracellular compartment (index "i"), the restricted subsarcolemal space (index "d"), and the uptake and release compartments of the sarcoplasmic reticulum (indices "up" and "rel" respectively); 14 gating variables: m, h_1, h_2, d_L, f_{L_1}, f_{L_2}, r, s, r_sus, s_sus, n, p_a, F_1, F_2; 5 buffer concentrations: O_C, O_TC, O_TMgC, O_TMgMg, O_Calse. The ionic currents flowing between the different compartments are illustrated in Fig. 3. The evolution equations are listed in Appendix Appendix B.

In the Nygren model, by analogy with Eq. (24), the non-specific charge $Q_{\rm ns}$ is *defined* as

$$\begin{aligned} Q_{\rm ns} = -C_m V + V_{\rm i} F \Big(& [{\rm Na}^+]_{\rm i} + [{\rm K}^+]_{\rm i} + 2\,[{\rm Ca}^{++}]_{\rm i} \\ & + 2\,(0.08\,O_{\rm TC} + 0.16\,O_{\rm TMgC} + 0.045\,O_{\rm C}) \Big) \\ & + 2V_{\rm d} F\,[{\rm Ca}^{++}]_{\rm d} + 2V_{\rm up} F\,[{\rm Ca}^{++}]_{\rm up} + 2V_{\rm rel} F\,([{\rm Ca}^{++}]_{\rm rel} + 31\,O_{\rm Calse}) \quad . \end{aligned} \tag{27}$$

In contrast with the Courtemanche model, this charge is not conserved, since after differentiating Eq. (27), it is found that

$$\frac{{\rm d}Q_{\rm ns}}{{\rm d}t} = -\Phi_{\rm Na,en} \quad . \tag{28}$$

As a result, no fixed point can exist in the original Nygren model unless $\Phi_{\rm Na,en} = 0$, because $Q_{\rm ns}$ remains constant in a steady-state. In the sequel, we will assume $\Phi_{\rm Na,en} = 0$. A motivation for using this assumption is given in subsection 7.1. Similarly to the Courtemanche model [Eq. (26)], $[{\rm NS}]_{\rm i}$ is defined by the relation $Q_{\rm ns} = V_{\rm i} F\,[{\rm NS}]_{\rm i}$.

4. Steady-state solutions in the Courtemanche model

In this section, it is shown that, for all $\overline{V} \leq +65$ mV, there exists a unique steady-state solution to the Courtemanche equations with a transmembrane potential $V(t) = \overline{V}$. So let us fix the value $\overline{V}$. The steady state value of all other state variables is determined as a function of $\overline{V}$.

4.1. Steady state equations

The steady state value of the gating variables are obtained from Eq. (7). The values of $\overline{m}$, $\overline{h}$, $\overline{j}$, $\overline{o_a}$, $\overline{o_i}$, $\overline{u_a}$, $\overline{u_i}$, $\overline{x_r}$, $\overline{x_s}$, $\overline{d}$, $\overline{f}$ and $\overline{w}$ are functions of $\overline{V}$ only and can be considered as constants for the steady state treated in this section. The gating variable $\overline{f}_{\rm Ca}$ is given by

$$\overline{f}_{\rm Ca} = \frac{1}{1 + \overline{[{\rm Ca}^{++}]}_{\rm i} \Big/ 3.5 \cdot 10^{-4}} \tag{29}$$

The variables $\overline{u}$ and $\overline{v}$ require a special attention and are treated in subsection 4.3.

The steady state currents have to satisfy the following relations derived by setting the time derivatives to zero in Eqs. (A.11)–(A.16):

$$\overline{I}_{\mathrm{Na,t}} = -3\,\overline{I}_{\mathrm{NaCa}} - 3\,\overline{I}_{\mathrm{NaK}} \tag{30}$$

$$\overline{I}_{\mathrm{K,t}} = 2\,\overline{I}_{\mathrm{NaK}} \tag{31}$$

$$\overline{I}_{\mathrm{Ca,t}} = 2\,\overline{I}_{\mathrm{NaCa}} \tag{32}$$

$$\overline{I}_{\mathrm{tr}} = (\overline{I}_{\mathrm{up}} - \overline{I}_{\mathrm{leak}})\,\frac{V_{\mathrm{up}}}{V_{\mathrm{rel}}} \tag{33}$$

$$\overline{I}_{\mathrm{rel}} = \overline{I}_{\mathrm{tr}} \quad . \tag{34}$$

In Eq. (32), the contributions of $\overline{I}_{\mathrm{tr}}$ and $\overline{I}_{\mathrm{rel}}$ have been cancelled by a linear combination with Eqs. (33) and (34). The equation $\overline{I}_{\mathrm{ion}} = 0$ resulting from Eq. (A.11) is automatically satisfied since it is equivalent to the sum of Eqs. (30)–(32).

The strategy for solving these equations is as follows. Equations (30) and (32) give two relations between $\overline{[\mathrm{Ca}^{++}]}_{\mathrm{i}}$ and $\overline{[\mathrm{Na}^{+}]}_{\mathrm{i}}$ which can be solved by substitution. Then, Eq. (31) provides an expression relating $\overline{[\mathrm{K}^{+}]}_{\mathrm{i}}$ and $\overline{[\mathrm{Na}^{+}]}_{\mathrm{i}}$. Finally, Eqs. (33)–(34) enable us to compute the variables associated with the sarcoplasmic reticulum.

First, the steady state ionic currents have to be evaluated. If the steady state values of the gating variables are introduced and the voltage dependent-functions are merged, the steady-state membrane currents are:

$$\overline{I}_{\mathrm{Na,t}} = \overline{g}_{\mathrm{Na,t}} \cdot (\overline{V} - \overline{E}_{\mathrm{Na}}) \tag{35}$$

$$\overline{I}_{\mathrm{K,t}} = \overline{g}_{\mathrm{K,t}} \cdot (\overline{V} - \overline{E}_{\mathrm{K}}) \tag{36}$$

$$\overline{I}_{\mathrm{Ca,t}} = \frac{I_{\mathrm{pCa,max}}}{1 + 5 \cdot 10^{-4} \Big/ \overline{[\mathrm{Ca}^{++}]}_{\mathrm{i}}} - \frac{\overline{I}_{\mathrm{CaL,min}}}{1 + \overline{[\mathrm{Ca}^{++}]}_{\mathrm{i}} \Big/ 3.5 \cdot 10^{-4}} + g_{\mathrm{bCa}} \cdot \left(\overline{V} - \overline{E}_{\mathrm{Ca}}\right) \tag{37}$$

$$\overline{I}_{\mathrm{NaCa}} = \overline{a} \cdot \overline{[\mathrm{Na}^{+}]}_{\mathrm{i}}^{3} - \overline{b} \cdot \overline{[\mathrm{Ca}^{++}]}_{\mathrm{i}} \tag{38}$$

$$\overline{I}_{\mathrm{NaK}} = \frac{\overline{I}_{\mathrm{NaK,max}}}{1 + \left(K_{\mathrm{m,Na}} \Big/ \overline{[\mathrm{Na}^{+}]}_{\mathrm{i}}\right)^{3/2}} \quad , \tag{39}$$

where $\overline{g}_{\mathrm{Na,t}}$, $\overline{g}_{\mathrm{K,t}}$, $\overline{I}_{\mathrm{CaL,min}}$, $\overline{I}_{\mathrm{NaK,max}}$, $\overline{a}$ and $\overline{b}$ are positive functions of $\overline{V}$, which do not depend

on the intracellular ionic concentrations. Note that $\overline{I}_{\mathrm{CaL,min}} = g_{\mathrm{CaL}} \cdot \overline{d} \cdot \overline{f} \cdot (65 - \overline{V}) > 0$ provided that $\overline{V} < 65$ mV.

4.2. Steady-state intracellular ionic concentrations

After insertion of Eqs. (35), (38) and (39) in Eq. (30), the steady state $[\mathrm{Ca}^{++}]_{\mathrm{i}}$ concentration is derived from the corresponding $[\mathrm{Na}^{+}]_{\mathrm{i}}$ concentration

$$3\,\overline{b} \cdot \overline{[\mathrm{Ca}^{++}]_{\mathrm{i}}} = 3\,\overline{a} \cdot \overline{[\mathrm{Na}^{+}]_{\mathrm{i}}}^{3} + \overline{g}_{\mathrm{Na,t}} \cdot (\overline{V} - \overline{E}_{\mathrm{Na}}) + \frac{3\,\overline{I}_{\mathrm{NaK,max}}}{1 + \left(K_{\mathrm{m,Na}} \Big/ \overline{[\mathrm{Na}^{+}]_{\mathrm{i}}} \right)^{3/2}} \quad . \tag{40}$$

Each term of the right hand side is an increasing function of $\overline{[\mathrm{Na}^{+}]_{\mathrm{i}}}$. When $\overline{[\mathrm{Na}^{+}]_{\mathrm{i}}} \to +\infty$, $\overline{[\mathrm{Ca}^{++}]_{\mathrm{i}}} \to +\infty$, whereas when $\overline{[\mathrm{Na}^{+}]_{\mathrm{i}}} \to 0$, $\overline{[\mathrm{Ca}^{++}]_{\mathrm{i}}} \to -\infty$ because of the logarithmic dependence in $\overline{E}_{\mathrm{Na}}$. Thus there is a critical intracellular sodium concentration $[\mathrm{Na}^{+}]_{\mathrm{i,crit}}$ below which no steady-state solution exists because then $\overline{[\mathrm{Ca}^{++}]_{\mathrm{i}}}$ would be negative.

If Eqs. (37) and (38) are substituted in Eq. (32), the following function is assembled

$$F_{\mathrm{Na}}\left(\overline{[\mathrm{Na}^{+}]_{\mathrm{i}}}\right) = 2\,\overline{b} \cdot \overline{[\mathrm{Ca}^{++}]_{\mathrm{i}}} - 2\,\overline{a} \cdot \overline{[\mathrm{Na}^{+}]_{\mathrm{i}}}^{3} + \frac{I_{\mathrm{pCa,max}}}{1 + 5 \cdot 10^{-4} \Big/ \overline{[\mathrm{Ca}^{++}]_{\mathrm{i}}}} - \frac{\overline{I}_{\mathrm{CaL,min}}}{1 + \overline{[\mathrm{Ca}^{++}]_{\mathrm{i}}} \Big/ 3.5 \cdot 10^{-4}} + g_{\mathrm{bCa}} \cdot \left(\overline{V} - \overline{E}_{\mathrm{Ca}}\right) \quad , \tag{41}$$

whose zeros are the steady-state values of $[\mathrm{Na}^{+}]_{\mathrm{i}}$. In this expression, $\overline{[\mathrm{Ca}^{++}]_{\mathrm{i}}}$ is a function of $\overline{[\mathrm{Na}^{+}]_{\mathrm{i}}}$, as derived in Eq. (40). This function is also increasing: the sum of the two first terms is increasing by Eq. (40) and the three last terms are increasing functions of $\overline{[\mathrm{Ca}^{++}]_{\mathrm{i}}}$, which in turn is an increasing function of $\overline{[\mathrm{Na}^{+}]_{\mathrm{i}}}$. Moreover, when $\overline{[\mathrm{Na}^{+}]_{\mathrm{i}}} \to [\mathrm{Na}^{+}]_{\mathrm{i,crit}}$, $F_{\mathrm{Na}} \to -\infty$ because of the term involving $\overline{E}_{\mathrm{Ca}}$, while when $\overline{[\mathrm{Na}^{+}]_{\mathrm{i}}} \to +\infty$, $F_{\mathrm{Na}} \to +\infty$. Therefore, there always exists a unique zero $\overline{[\mathrm{Na}^{+}]_{\mathrm{i}}}$ of the function F_{Na}.

First, the value of $[\mathrm{Na}^{+}]_{\mathrm{i,crit}}$ is determined by solving Eq. (40) numerically for $\overline{[\mathrm{Ca}^{++}]_{\mathrm{i}}} = 0$ in the interval $(0, +\infty)$. Second, the zero of F_{Na} is found in the interval $([\mathrm{Na}^{+}]_{\mathrm{i,crit}}, +\infty)$. For the required root-finding procedure, the false position method (regula falsi) was used.

The potassium concentration $\overline{[\mathrm{K}^+]}_\mathrm{i}$ is obtained from Eq. (31)

$$\overline{[\mathrm{K}^+]}_\mathrm{i} = [\mathrm{K}^+]_\mathrm{o} \ \exp\left[\frac{F}{RT}\left(\frac{2\overline{I}_\mathrm{NaK}}{\overline{g}_\mathrm{K,t}} - \overline{V}\right)\right] \quad , \tag{42}$$

where $\overline{I}_\mathrm{NaK}$ is computed from Eq. (39), using the obtained value of $\overline{[\mathrm{Na}^+]}_\mathrm{i}$ obtained just above.

4.3. Calcium dynamics at steady-state

Once the intracellular ionic concentrations are known, only $\overline{[\mathrm{Ca}^{++}]}_\mathrm{rel}$, $\overline{[\mathrm{Ca}^{++}]}_\mathrm{up}$, $\overline{u}$ and $\overline{v}$ remain to be determined. Note that, in this case, $\overline{I}_\mathrm{up}$ becomes a constant and $\overline{I}_\mathrm{leak} = \alpha \cdot \overline{[\mathrm{Ca}^{++}]}_\mathrm{up}$ where α is defined as $I_\mathrm{up,max}/[\mathrm{Ca}^{++}]_\mathrm{up(max)}$.

The concentration $\overline{[\mathrm{Ca}^{++}]}_\mathrm{up}$ is expressed as a function of $\overline{[\mathrm{Ca}^{++}]}_\mathrm{rel}$ using Eqs. (33) and (A.9)

$$\overline{[\mathrm{Ca}^{++}]}_\mathrm{up} = \frac{\tau_\mathrm{tr}\beta\overline{I}_\mathrm{up} + \overline{[\mathrm{Ca}^{++}]}_\mathrm{rel}}{1 + \alpha\beta\tau_\mathrm{tr}} \quad , \tag{43}$$

where β is defined as the ratio $V_\mathrm{up}/V_\mathrm{rel}$. As a result, from Eq. (34), we have

$$\overline{I}_\mathrm{tr} \ = \ \frac{\beta\overline{I}_\mathrm{up} - \alpha\beta\,\overline{[\mathrm{Ca}^{++}]}_\mathrm{rel}}{1 + \alpha\beta\tau_\mathrm{tr}} \ = \ \overline{I}_\mathrm{rel} \ = \ k_\mathrm{rel}\,\overline{u}^2\overline{v}\,\overline{w}\left(\overline{[\mathrm{Ca}^{++}]}_\mathrm{rel} - \overline{[\mathrm{Ca}^{++}]}_\mathrm{i}\right) \quad . \tag{44}$$

This equation can be written as

$$\frac{\overline{I}_\mathrm{up} - \alpha\,\overline{[\mathrm{Ca}^{++}]}_\mathrm{rel}}{\overline{[\mathrm{Ca}^{++}]}_\mathrm{rel} - \overline{[\mathrm{Ca}^{++}]}_\mathrm{i}} = A\,\overline{u}^2\overline{v} \quad , \tag{45}$$

where $A = k_\mathrm{rel}\,\overline{w}(1 + \alpha\beta\tau_\mathrm{tr})/\beta$ depends only on $\overline{V}$. For the right hand side to be positive, $\overline{[\mathrm{Ca}^{++}]}_\mathrm{rel}$ has to lie within the interval bounded by $\overline{[\mathrm{Ca}^{++}]}_\mathrm{i}$ and $\overline{I}_\mathrm{up}/\alpha$. In this interval, the left hand side is a monotonic function of $\overline{[\mathrm{Ca}^{++}]}_\mathrm{rel}$, denoted by $F_\mathrm{rel}(\overline{[\mathrm{Ca}^{++}]}_\mathrm{rel})$, whose range is $[0, +\infty)$, and whose derivative (in absolute value) is bounded from below:

$$\left|F'_\mathrm{rel}(\overline{[\mathrm{Ca}^{++}]}_\mathrm{rel})\right| \ \geq \ \left|F'_\mathrm{rel}(\overline{I}_\mathrm{up}/\alpha)\right| \ = \ \frac{\alpha^2}{\left|\overline{I}_\mathrm{up} - \alpha\overline{[\mathrm{Ca}^{++}]}_\mathrm{i}\right|} \ \geq \ \frac{\alpha^2}{I_\mathrm{up,max} + \alpha\overline{[\mathrm{Ca}^{++}]}_\mathrm{i}} \quad . \tag{46}$$

Since $A\,\overline{u}^2\overline{v} \geq 0$, Eq. (45) has at least one solution. In order to prove the uniqueness of this solution, we will show that $F_\mathrm{rel}(\overline{[\mathrm{Ca}^{++}]}_\mathrm{rel}) - A\,\overline{u}^2\overline{v}$ is a monotonic function of $\overline{[\mathrm{Ca}^{++}]}_\mathrm{rel}$. For

this purpose, the slope of $A\,\overline{u}^2\overline{v}$ (in absolute value) will be shown to be always much smaller than that of $F_{\rm rel}$. Note that $\overline{u}^2\overline{v}$ is implicitly a function of $\overline{[{\rm Ca}^{++}]}_{\rm rel}$. More precisely,

$$\overline{u} \;=\; u_\infty\left(\overline{F}_n\right) \;=\; \left[1+\exp\left(-\frac{\overline{F}_n-0.34175}{\Delta F_n}\right)\right]^{-1} \tag{47}$$

$$\overline{v} \;=\; v_\infty\left(\overline{F}_n\right) \;=\; \left[1+\exp\left(+\frac{\overline{F}_n-0.06835}{\Delta F_n}\right)\right]^{-1} \quad , \tag{48}$$

where $\Delta F_n = 1.367\cdot 10^{-3}$ and the $\overline{F}_n$ is given by [2]

$$\overline{F}_n = V_{\rm rel}\overline{I}_{\rm rel} - \frac{1}{2F}\left(\frac{1}{2}\overline{I}_{\rm CaL} - \frac{1}{5}\overline{I}_{\rm NaCa}\right) \quad . \tag{49}$$

By Eq. (44), $\overline{F}_n$ is an affine function of $\overline{[{\rm Ca}^{++}]}_{\rm rel}$.

The right hand side of Eq. (45) has a derivative (in absolute value) that can be bounded from above:

$$\left|\frac{{\rm d}(A\overline{u}^2\overline{v})}{{\rm d}\overline{F}_n}\right| \;\le\; \frac{3A\,\overline{u}^2\overline{v}}{\Delta F_n} \qquad \text{and hence} \qquad \left|\frac{{\rm d}(A\overline{u}^2\overline{v})}{{\rm d}\overline{[{\rm Ca}^{++}]}_{\rm rel}}\right| \;\le\; \frac{3\alpha k_{\rm rel}V_{\rm rel}\,\overline{u}^2\overline{v}\overline{w}}{\Delta F_n} \tag{50}$$

using Eqs. (44), (49), and the relation ${\rm d}\overline{u}/{\rm d}\overline{F}_n = -\overline{u}(1-\overline{u})/\Delta F_n$. This upper bound is actually very small because

$$\overline{u}^2\overline{v} \;\le\; \overline{u}\,\overline{v} \;\le\; \max_{F_n}\; u_\infty(F_n)v_\infty(F_n) \;\approx\; 1.4\cdot 10^{-87} \quad , \tag{51}$$

where the maximum is reached at $F_n = (0.34175+0.06835)/2$. For the physiological values of the model parameters given in [2], the ratio of the maximum slope of $A\overline{u}^2\overline{v}$ [Eqs. (50)-(51)] and the minimum slope of $F_{\rm rel}$ [Eq. (46)] is bounded by a small (dimensionless) quantity

$$\frac{3k_{\rm rel}V_{\rm rel}\,\overline{u}^2\overline{v}\,\overline{w}\;\left(I_{\rm up,max}+\alpha\overline{[{\rm Ca}^{++}]}_{\rm i}\right)}{\alpha\,\Delta F_n} \;<\; 10^{-77} \quad , \tag{52}$$

assuming $\overline{[{\rm Ca}^{++}]}_{\rm i} < 1000$ mM. Therefore, $F_{\rm rel}(\overline{[{\rm Ca}^{++}]}_{\rm rel}) - A\,\overline{u}^2\overline{v}$ is a monotonic function and Eq. (45) has exactly one solution. This solution $\overline{[{\rm Ca}^{++}]}_{\rm rel}$ can be determined by solving numerically Eq. (45), in which $\overline{u}^2\overline{v}$ is obtained from Eqs. (47)–(49) and (44). The concentration $\overline{[{\rm Ca}^{++}]}_{\rm up}$ is then obtained from Eq. (43), and the steady-state flux $\overline{F}_n$ from Eq. (49). Finally, Eqs. (47)–(48) are used to evaluate $\overline{u}$ and $\overline{v}$.

A very accurate approximation can be derived by neglecting $\overline{u}^2\overline{v}$ in Eq. (45). Under this assumption,

$$\overline{[\mathrm{Ca}^{++}]}_{\mathrm{rel}} \;\approx\; \overline{[\mathrm{Ca}^{++}]}_{\mathrm{up}} \;\approx\; \frac{\overline{I}_{\mathrm{up}}}{\alpha} \;=\; \frac{[\mathrm{Ca}^{++}]_{\mathrm{up,max}}}{1 + K_{\mathrm{up}} \Big/ \overline{[\mathrm{Ca}^{++}]}_{\mathrm{i}}} \quad , \tag{53}$$

where the error is $\mathcal{O}(\overline{u}^2\overline{v})$.

4.4. Graphical representation of the steady states

Using the formulas given in the previous subsections, the steady states were computed for values of $\overline{V}$ ranging from -90 to 0 mV. The accuracy of the results was checked by testing if $\|\mathbf{f}(\overline{\mathbf{x}})\|$ was sufficiently small [Eq. (6)]. The stability of the steady states was established using Eq. (11). The main state variables were represented as a function of the non-specific charge concentration $[\mathrm{NS}]_{\mathrm{i}}$. The value of $[\mathrm{NS}]_{\mathrm{i}}$ remains constant over time and is therefore associated with the choice of an initial condition. The initial condition proposed for the original model corresponds to that computed for $\overline{V} = -81.2$ mV and is associated with the physiological value $[\mathrm{NS}]_{\mathrm{i}} = 150.2$ mM.

For all fixed points, the steady-state transmembrane potential as well as the main intracellular ionic concentrations are displayed in Fig. 4, solid lines corresponding to stable fixed points and dashed lines to unstable ones. Four regimes were observed: there was a single stable fixed point for $[\mathrm{NS}]_{\mathrm{i}} < 53$ mM, an unstable fixed point in the interval $53 < [\mathrm{NS}]_{\mathrm{i}} < 93$ mM, one stable and two unstable fixed points in the interval $93 < [\mathrm{NS}]_{\mathrm{i}} < 117$ mM, and a single stable fixed point for $[\mathrm{NS}]_{\mathrm{i}} > 117$ mM. The unstable fixed points were found for transmembrane potentials $\overline{V}$ between -54.7 and -24.5 mV.

5. Dynamical Regimes in the Courtemanche model

Since $[\mathrm{NS}]_{\mathrm{i}}$ is an invariant of the dynamics, the system evolves toward a stable fixed point (attractor) with a value of $[\mathrm{NS}]_{\mathrm{i}}$ corresponding to that of the initial condition. In the absence of any stable fixed point, the system is expected to tend toward a stable limit cycle (pacemaker

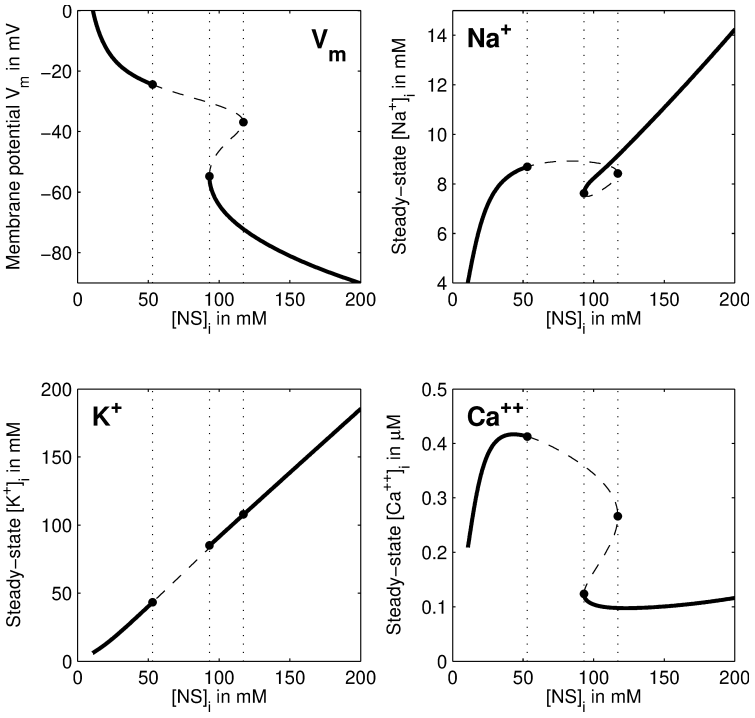

Figure 4: Steady-state transmembrane potential and intracellular ionic concentrations for all fixed points of the Courtemanche model, represented as a function of the non-specific charge concentration $[NS]_i$. Solid lines mean stable fixed points and dashed lines unstable fixed points. The vertical dotted lines denote the transitions between different dynamical regimes.

activity). In order to study the far-from-equilibrium dynamics, the effect of large perturbation was studied by applying external stimulation.

5.1. System with external stimulation

When a stimulation current is applied, Eq. (A.11) is replaced by [1]

$$C_m \frac{\mathrm{d}V}{\mathrm{d}t} = -I_{\mathrm{Na,t}} - I_{\mathrm{K,t}} - I_{\mathrm{Ca,t}} - I_{\mathrm{NaCa}} - I_{\mathrm{NaK}} + I_{\mathrm{stim}}(t) \quad , \tag{54}$$

where I_{stim} is the stimulation current ($I_{\mathrm{stim}} > 0$ induces a depolarization). In this case, Eq. (25) is not valid anymore and the current I_{stim} contributes to changes in the non-specific charge concentration [18]

$$[\mathrm{NS}]_{\mathrm{i}}(t) = [\mathrm{NS}]_{\mathrm{i}}(0) - \frac{1}{V_{\mathrm{i}} F} \int_0^t \mathrm{d}\tau \; I_{\mathrm{stim}}(\tau) \quad . \tag{55}$$

The drift expressed by the integral is not desirable since the qualitative behavior of the cell dynamics can be altered when the value of $[\mathrm{NS}]_{\mathrm{i}}$ is changed. In order to restore the conservation of $[\mathrm{NS}]_{\mathrm{i}}$, a charge carrier has to be chosen for the stimulation current. Following Hund *et al.* [8], the potassium was considered to be the only ion whose concentration is affected by the stimuli, so that Eq. (A.13) is replaced by

$$\frac{\mathrm{d}[\mathrm{K}^+]_{\mathrm{i}}}{\mathrm{d}t} = \frac{2I_{\mathrm{NaK}} - I_{\mathrm{K,t}} + I_{\mathrm{stim}}(t)}{F V_{\mathrm{i}}} \quad . \tag{56}$$

This equation is used when simulating the action potentials documented in the next subsection.

5.2. Response to large perturbations

A simulation was performed for a representative selection of fixed points, starting from the fixed point as initial condition. After 250 ms of free evolution, a stimulus of amplitude 2 nA was applied for 2 ms. This current was carried by the potassium ions [Eq. (56)]. To ensure the exact conservation of $[\mathrm{NS}]_{\mathrm{i}}$, $[\mathrm{K}^+]_{\mathrm{i}}$ was computed at each time step using Eq. (24), following an approach similar to the algebraic integration scheme described in Hund *et al.* [8].

Figure 5 illustrates the four regimes observed. During the first 250 ms of free evolution, the transmembrane potential seems to be stable even around an unstable fixed point. This is due to the fact that the fixed point was accurately computed and the Lyapunov exponent was small. The exponential divergence of the trajectory follows $\|\mathbf{x}(t) - \overline{\mathbf{x}}\| \approx \|\mathbf{x}(0) - \overline{\mathbf{x}}\| \exp(\lambda t)$, where λ is the Lyapunov exponent, whose value was found to be around 0.01 ms^{-1}. With an accurate estimate of the fixed point, for instance, $\|\mathbf{x}(0) - \overline{\mathbf{x}}\| \approx 10^{-8} \|\overline{\mathbf{x}}\|$, the state of the system is still very close to the fixed point after 250 ms of free evolution. For $[\text{NS}]_\text{i} < 53$ mM, a stable fixed point exists with a high resting potential, but the system is not excitable (the electrical response of the cell is similar to a passive cell). In the interval $53 < [\text{NS}]_\text{i} < 93$ mM, there is only an unstable fixed point and the dynamics is auto-oscillatory with a cycle length ranging between 520 and 1200 ms (the larger $[\text{NS}]_\text{i}$, the slower the firing rate). In the interval $93 < [\text{NS}]_\text{i} < 117$ mM, three fixed points exist, one of which is stable. For $[\text{NS}]_\text{i} > 117$ mM, these is a single stable fixed point. A superthreshold stimulation generates an action potential with a duration between 230 and 350 ms measured at 90% repolarization For decreasing values of $[\text{NS}]_\text{i}$, the resting potential becomes elevated, the action potential duration prolongs and the notch progressively disappears.

6. Steady-state solutions in the Nygren model

In this section, it is shown that, in case $\Phi_{\text{Na,en}} = 0$, for all $\overline{V} \geq -150$ mV, one, two or three steady-state solutions to the Nygren equations exist for a transmembrane potential $V(t) = \overline{V}$. The steady state value of all the other state variables is determined as a function of $\overline{V}$.

6.1. Steady-state equations

First of all, the steady state value of the gating variables are obtained from Eq. (7). The values of $\overline{m}$, $\overline{h_1}$, $\overline{h_2}$, $\overline{d_L}$, $\overline{f_{L_1}}$, $\overline{f_{L_2}}$, $\overline{r}$, $\overline{s}$, $\overline{r_{\text{sus}}}$, $\overline{s_{\text{sus}}}$, $\overline{n}$ and $\overline{p_a}$ are functions of $\overline{V}$ and can therefore be considered as constants within this section [3]. The gating variables f_{Ca}, F_1 and F_2 are considered later because they depend on $[\text{Ca}^{++}]_\text{i}$ and $[\text{Ca}^{++}]_\text{d}$ (see [3]). By setting the time

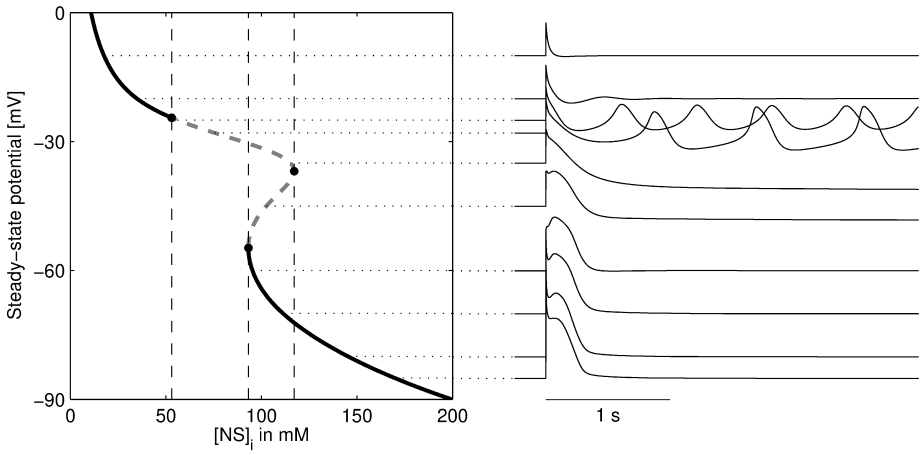

Figure 5: Steady states of the Courtemanche model. *Left panel*: transmembrane potential of the fixed points as a function of the non-specific charge concentration $[\mathrm{NS}]_\mathrm{i}$. The display correspond to that of Fig. 4. *Right panel*: time course of the transmembrane potential starting from the initial condition indicated by the horizontal dotted line.

derivatives in Eqs. (B.15)–(B.21) to zero, the steady state currents can be shown to satisfy the following relations:

$$3\overline{I}_{\mathrm{NaCa}} = -3\overline{I}_{\mathrm{NaK}} - \overline{I}_{\mathrm{Na,t}} \tag{57}$$

$$2\overline{I}_{\mathrm{NaK}} = \overline{I}_{\mathrm{K,t}} \tag{58}$$

$$\overline{I}_{\mathrm{di}} = -\overline{I}_{\mathrm{CaL}} \tag{59}$$

$$\overline{I}_{\mathrm{Ca,t}} = 2\overline{I}_{\mathrm{NaCa}} + \overline{I}_{\mathrm{di}} \tag{60}$$

$$\overline{I}_{\mathrm{up}} = \overline{I}_{\mathrm{tr}} = \overline{I}_{\mathrm{rel}} \ . \tag{61}$$

Equations (57) and (60) yield two relations between $\overline{[\mathrm{Na}^+]}_\mathrm{i}$ and $\overline{[\mathrm{Ca}^{++}]}_\mathrm{i}$, Eq. (58) a relation between $\overline{[\mathrm{K}^+]}_\mathrm{i}$ and $\overline{[\mathrm{Na}^+]}_\mathrm{i}$, and Eq. (59) a relation between $\overline{[\mathrm{Ca}^{++}]}_\mathrm{d}$ and $\overline{[\mathrm{Ca}^{++}]}_\mathrm{i}$. Equation (61) enables us to determine the variables associated with the sarcoplasmic reticulum.

6.2. Steady-state ionic concentrations

After having introduced Eqs. (57)–(61) in Eqs. (B.22)–(B.24), the steady-state cleft concentrations are found to be equal to the bulk concentrations:

$$\overline{[\mathrm{K}^+]}_\mathrm{c} = [\mathrm{K}^+]_\mathrm{b} \ , \quad \overline{[\mathrm{Na}^+]}_\mathrm{c} = [\mathrm{Na}^+]_\mathrm{b} \ , \quad \text{and} \quad \overline{[\mathrm{Ca}^{++}]}_\mathrm{c} = [\mathrm{Ca}^{++}]_\mathrm{b} \ . \tag{62}$$

Note that since $\overline{f_{L_1}} = \overline{f_{L_2}}$ (see [3]), $\overline{I}_\mathrm{CaL}$ is a function of $\overline{V}$ only because the dependency in f_Ca disappears at steady-state. Therefore, from the definition of I_di [Eq. (B.9)], we have

$$\overline{[\mathrm{Ca}^{++}]}_\mathrm{d} = \overline{[\mathrm{Ca}^{++}]}_\mathrm{i} - \frac{\tau_\mathrm{di}\,\overline{I}_\mathrm{CaL}}{2FV_\mathrm{d}} \ . \tag{63}$$

In order to determine $\overline{[\mathrm{Na}^+]}_\mathrm{i}$ and $\overline{[\mathrm{Ca}^{++}]}_\mathrm{i}$, we combine Eqs. (57) and (60). First, the current I_NaCa has the following form at steady state [Eq. (B.11)]:

$$\overline{I}_\mathrm{NaCa} = \frac{a\,\overline{[\mathrm{Na}^+]}_\mathrm{i}^3 - b\,\overline{[\mathrm{Ca}^{++}]}_\mathrm{i}}{1 + c\,\overline{[\mathrm{Na}^+]}_\mathrm{i}^3 + d\,\overline{[\mathrm{Ca}^{++}]}_\mathrm{i}} \tag{64}$$

where a, b, c and d are positive and depend only on $\overline{V}$ and on the cleft concentrations, which have already been determined. Next, we define $F_\mathrm{Na} = 3\overline{I}_\mathrm{NaK} + \overline{I}_\mathrm{Na,t}$ and $F_\mathrm{Ca} = \overline{I}_\mathrm{Ca,t} + \overline{I}_\mathrm{CaL}$, the former depending only on $[\mathrm{Na}^+]_\mathrm{i}$ and the latter on $[\mathrm{Ca}^{++}]_\mathrm{i}$. These functions are given by

$$\begin{aligned} F_\mathrm{Na}\left(\overline{[\mathrm{Na}^+]}_\mathrm{i}\right) &= \overline{g}_\mathrm{Na}\left(\mathrm{e}^{FV/RT}[\mathrm{Na}^+]_\mathrm{i} - [\mathrm{Na}^+]_\mathrm{b}\right) + g_\mathrm{bNa}\cdot(\overline{V} - \overline{E}_\mathrm{Na}) \\ &\quad + 3\overline{I}_\mathrm{NaK,max}\frac{[\mathrm{Na}^+]_\mathrm{i}^{3/2}}{[\mathrm{Na}^+]_\mathrm{i}^{3/2} + k_\mathrm{NaK,Na}^{3/2}} \end{aligned} \tag{65}$$

$$F_\mathrm{Ca}\left(\overline{[\mathrm{Ca}^{++}]}_\mathrm{i}\right) = \overline{I}_\mathrm{CaL} + \frac{I_\mathrm{pCa,max}}{1 + 5\cdot 10^{-4}\Big/\overline{[\mathrm{Ca}^{++}]}_\mathrm{i}} + g_\mathrm{bCa}\cdot(\overline{V} - \overline{E}_\mathrm{Ca}) \ , \tag{66}$$

where $\overline{g}_\mathrm{Na} = g_\mathrm{Na}(\overline{V})\cdot(0.9\,\overline{h_1} + 0.1\,\overline{h_2})$ and $\overline{I}_\mathrm{NaK,max} = I_\mathrm{NaK,max}\cdot[\mathrm{K}^+]_\mathrm{b}/(k_\mathrm{NaK,K} + [\mathrm{K}^+]_\mathrm{b})\cdot(\overline{V} + 150)/(\overline{V} + 200) \geq 0$ when $\overline{V} \geq -150$ mV. These functions are both increasing and tend toward $-\infty$ (resp. $+\infty$) when the argument tends toward 0 (resp. $+\infty$). From the relation $F_\mathrm{Na} = -3\overline{I}_\mathrm{NaCa}$ [Eq. (57)], the steady-state concentration $\overline{[\mathrm{Ca}^{++}]}_\mathrm{i}$ can be identified

$$\overline{[\mathrm{Ca}^{++}]}_\mathrm{i} = \frac{a\,\overline{[\mathrm{Na}^+]}_\mathrm{i}^3 + \frac{1}{3}\,F_\mathrm{Na}\left(\overline{[\mathrm{Na}^+]}_\mathrm{i}\right)\cdot\left(1 + c\,\overline{[\mathrm{Na}^+]}_\mathrm{i}^3\right)}{b - \frac{d}{3}\,F_\mathrm{Na}\left(\overline{[\mathrm{Na}^+]}_\mathrm{i}\right)} \ . \tag{67}$$

The value of $\overline{[\mathrm{Ca}^{++}]}_\mathrm{i}$ must be positive. This condition is verified if

$$-\frac{3a\,\overline{[\mathrm{Na}^+]}_\mathrm{i}^3}{1+c\,\overline{[\mathrm{Na}^+]}_\mathrm{i}^3} \;<\; F_\mathrm{Na}\left(\overline{[\mathrm{Na}^+]}_\mathrm{i}\right) \;<\; \frac{3b}{d} \quad . \tag{68}$$

Since the lower bound is a decreasing function of $\overline{[\mathrm{Na}^+]}_\mathrm{i}$ and F_Na is an increasing bijection from $(0,+\infty)$ to $(-\infty,+\infty)$, this condition can be written as

$$[\mathrm{Na}^+]_{\mathrm{i,crit}-} \;<\; [\mathrm{Na}^+]_\mathrm{i} \;<\; [\mathrm{Na}^+]_{\mathrm{i,crit}+} \quad , \tag{69}$$

where the bounds are well defined and can be easily computed numerically. Within this interval, $\overline{[\mathrm{Ca}^{++}]}_\mathrm{i}$ is the ratio between a positive increasing and a positive decreasing function. It is therefore an increasing function of $\overline{[\mathrm{Na}^+]}_\mathrm{i}$.

Then, using the relation $\overline{I}_\mathrm{NaCa} = \frac{1}{2}F_\mathrm{Ca} = -\frac{1}{3}F_\mathrm{Na}$ [Eq. (57) and (60)], we find that $\overline{[\mathrm{Na}^+]}_\mathrm{i}$ is a solution to the equation

$$3\,F_\mathrm{Ca}\left(\overline{[\mathrm{Ca}^{++}]}_\mathrm{i}\right) + 2\,F_\mathrm{Na}\left(\overline{[\mathrm{Na}^+]}_\mathrm{i}\right) = 0 \quad , \tag{70}$$

where $\overline{[\mathrm{Ca}^{++}]}_\mathrm{i}$ is the function of $\overline{[\mathrm{Na}^+]}_\mathrm{i}$ given by Eq. (67). The left hand side is an increasing function of $\overline{[\mathrm{Na}^+]}_\mathrm{i}$. It tends to $-\infty$ when $\overline{[\mathrm{Na}^+]}_\mathrm{i} \to [\mathrm{Na}^+]_{\mathrm{i,crit}-}$ because $\overline{[\mathrm{Ca}^{++}]}_\mathrm{i} \to 0$, and it tends to $+\infty$ when $\overline{[\mathrm{Na}^+]}_\mathrm{i} \to [\mathrm{Na}^+]_{\mathrm{i,crit}+}$ because the denominator in Eq. (67) becomes zero. Thus, the solution $\overline{[\mathrm{Na}^+]}_\mathrm{i}$ to Eq. (70) exists, is unique and can be easily computed using a numerical root-finding algorithm in the open interval between $[\mathrm{Na}^+]_{\mathrm{i,crit}-}$ and $[\mathrm{Na}^+]_{\mathrm{i,crit}+}$. The value of $\overline{[\mathrm{Ca}^{++}]}_\mathrm{i}$ is finally derived from Eq. (67) and the value of $\overline{[\mathrm{Ca}^{++}]}_\mathrm{d}$ from Eq. (63).

The next step is to determine $\overline{[\mathrm{K}^+]}_\mathrm{i}$. This is done by solving Eq. (58). After having substituted the formula of $g_\mathrm{K1}(V)$ (see [3]), this equation becomes

$$\overline{g}_\mathrm{K1}[\mathrm{K}^+]_\mathrm{b}^{0.4457}\frac{\overline{V}-\overline{E}_\mathrm{K}}{1+\exp\left(1.5(\overline{V}-\overline{E}_\mathrm{K}+3.6)F/RT\right)} + \overline{g}_\mathrm{K,tot}\cdot(\overline{V}-\overline{E}_\mathrm{K}) = 2\overline{I}_\mathrm{NaK} \quad , \tag{71}$$

where the equivalent conductance $\overline{g}_\mathrm{K,tot}$ is defined as $g_\mathrm{t}\overline{r}\,\overline{s} + g_\mathrm{sus}\overline{r_\mathrm{sus}}\,\overline{s_\mathrm{sus}} + \overline{g}_\mathrm{Kr}\overline{p_a} + \overline{g}_\mathrm{Ks}\overline{n}$, and where the current $\overline{I}_\mathrm{NaK}$ is computed with the value of $\overline{[\mathrm{Na}^+]}_\mathrm{i}$ determined previously. This is

an equation for $x = \overline{V} - \overline{E}_{\mathrm{K}}$, which has one, two or three solutions, as is shown in the next subsection. For each possible value of x, the potassium concentration is then computed as

$$\overline{[\mathrm{K}^+]}_{\mathrm{i}} = [\mathrm{K}^+]_{\mathrm{b}} \, \exp\left(\frac{(x - \overline{V})F}{RT}\right) \quad . \tag{72}$$

Once the intracellular concentrations are known, this leaves us the variables of the sarcoplasmic reticulum and the buffer concentrations to be found, as is done in subsections 6.4 and 6.5.

6.3. Solving the potassium equation

The equation for computing $\overline{[\mathrm{K}^+]}_{\mathrm{i}}$ is of the form (see Eq. (71) and Fig. 6)

$$f(x) = \frac{x}{1 + \exp(ax + b)} = c - rx \tag{73}$$

where the first equality is a definition and $x = \overline{V} - \overline{E}_{\mathrm{K}}$. The parameters a, b, c and r are all positive. We will see that under this assumption this equation has 1, 2 or 3 roots and sketch how to compute all of them numerically. Since the roots are clearly in the interval $(0, c/r)$, we assume that $x \geq 0$. The function f and its derivative f' are plotted in Fig. 6.

The function f has a unique local maximum (x_m such that $f'(x_m) = 0$) at

$$x_m = \frac{1 + W\big(\exp(-b - 1)\big)}{a} \tag{74}$$

where W is the Lambert's W function [16]. An inflexion point x_i of f is a solution to $f''(x_i) = 0$, which is equivalent to

$$\exp(ax + b) = \frac{ax + 2}{ax - 2} \quad . \tag{75}$$

The right hand side is negative for $|x| < 2/a$, positive and decreasing for $x > 2/a$, while the left hand side is positive and increasing. Therefore there exists a unique inflexion point x_i lying in the interval $(2/a, +\infty)$.

In order to determine the number of roots, we need to find the points such that $f'(x) = -r$ (see Fig. 6). This equation has no solution if $f'(x_i) > -r$. In this case, Eq. (73) has a unique root in the interval $(0, c/r)$. If $f'(x_i) < -r$, then $f'(x) = -r$ has two solutions x_1 and

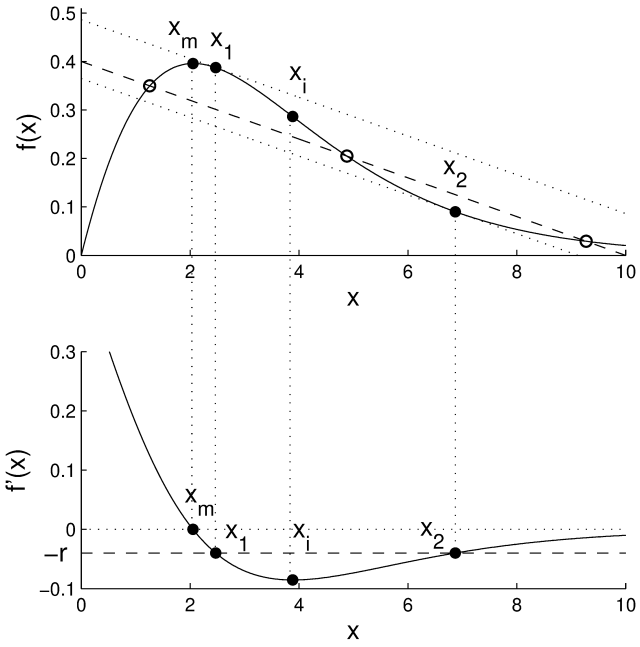

Figure 6: The function f (top panel) and its derivative f' (bottom panel) are represented for $a = 0.6$, $b = 0.2$, $c = 0.4$ and $r = 0.04$. The points x_m, x_i, x_1 and x_2 are indicated on both graphs. On the top panel, the dashed line represents the equation $y = c - rx$. The circles indicate the solutions to Eq. (73). On the bottom panel, the horizontal dashed line $y = -r$ is also displayed.

x_2, the former being in the interval (x_m, x_i) and the latter in $(x_i, +\infty)$. Next, we define $c_1 = f(x_1) + rx_1$ and $c_2 = f(x_2) + rx_2$. Equation (73) has a unique solution in $(0, c/r)$ if $c > c_2$ or $c < c_1$, two solutions if $c = c_1$ (one is x_1 and the other one is in $(x_1, c/r)$), two solutions if $c = c_2$ (one is x_2 and the other one is in $(0, x_2)$), three solutions if $c_1 < c < c_2$ (one in $(0, x_1)$, in (x_1, x_2) and in $(x_2, c/r)$). In the degenerate case $f'(x_i) = -r$, Eq. (73) always has a unique root in $(0, c/r)$.

6.4. Steady-state calcium dynamics

First, the steady-state values of F_1 and F_2 are derived from Eqs. (B.31)–(B.32):

$$\overline{F}_1 = \frac{1}{1 + \overline{r}_{\text{act}}/\overline{r}_{\text{inact}} + \overline{r}_{\text{act}}/\overline{r}_{\text{recov}}} \ , \qquad \overline{F}_2 = \frac{\overline{r}_{\text{act}}}{\overline{r}_{\text{inact}}} \, \overline{F}_1 \ , \tag{76}$$

where $\overline{r}_{\text{act}}$, $\overline{r}_{\text{inact}}$, and $\overline{r}_{\text{recov}}$ are computed from $\overline{[\text{Ca}^{++}]}_{\text{i}}$ and $\overline{[\text{Ca}^{++}]}_{\text{d}}$. From $\overline{I}_{\text{tr}} = \overline{I}_{\text{rel}}$ [Eqs. (61), (B.13) and (B.14)], an affine relation can be extracted between $\overline{[\text{Ca}^{++}]}_{\text{up}}$ and $\overline{[\text{Ca}^{++}]}_{\text{rel}}$:

$$\overline{[\text{Ca}^{++}]}_{\text{rel}} = a \cdot \overline{[\text{Ca}^{++}]}_{\text{up}} + b \qquad \text{where}$$
$$a = \left[1 + \frac{\alpha_{\text{rel}} \tau_{\text{tr}}}{2F V_{\text{rel}}} \left(\frac{\overline{F}_2}{\overline{F}_2 + 1/4} \right)^2 \right]^{-1} \qquad \text{and} \qquad b = (1-a) \cdot \overline{[\text{Ca}^{++}]}_{\text{i}} \ . \tag{77}$$

Then, the current I_{up} can be written as a function of $\overline{[\text{Ca}^{++}]}_{\text{up}}$,

$$\overline{I}_{\text{up}} = \frac{a_1 - b_1 \, \overline{[\text{Ca}^{++}]}_{\text{up}}}{a_2 + b_2 \, \overline{[\text{Ca}^{++}]}_{\text{up}}} \ , \tag{78}$$

where $a_1 = I_{\text{up,max}} \overline{[\text{Ca}^{++}]}_{\text{i}} / k_{\text{cyca}}$, $a_2 = 1 + \overline{[\text{Ca}^{++}]}_{\text{i}} / k_{\text{cyca}} + k_{\text{xcs}}^2 / k_{\text{srca}}$, $b_1 = I_{\text{up,max}} k_{\text{xcs}}^2 / k_{\text{cyca}}$ and $b_2 = k_{\text{xcs}} / k_{\text{srca}}$ are positive constants. From $\overline{I}_{\text{tr}} = \overline{I}_{\text{up}}$ [Eqs. (B.13), (77) and (78)], we have

$$c(1-a) b_2 \, \overline{[\text{Ca}^{++}]}_{\text{up}}^2 + \Big[b_1 + \big((1-a) a_2 - b_2 b \big) \Big] \, \overline{[\text{Ca}^{++}]}_{\text{up}} - a_2 b c - a_2 = 0 \ , \tag{79}$$

where $c = 2F V_{\text{rel}} / \tau_{\text{tr}}$. Since the leading coefficient is positive ($a < 1$ by its definition) and the constant term is negative, this quadratic equation has exactly one positive solution. Finally, $\overline{[\text{Ca}^{++}]}_{\text{rel}}$ is computed from $\overline{[\text{Ca}^{++}]}_{\text{up}}$ using Eq. (77).

6.5. Steady-state buffers

The equations for the calcium buffer concentration [Eqs. (B.25)–(B.29)] are similar to those of the gating variables. The steady state values of these variables read:

$$\overline{O}_{\mathrm{C}} = \frac{1}{1 + 2.38 \cdot 10^{-3} \Big/ \overline{[\mathrm{Ca}^{++}]}_{\mathrm{i}}} , \qquad \overline{O}_{\mathrm{TC}} = \frac{1}{1 + 5 \cdot 10^{-3} \Big/ \overline{[\mathrm{Ca}^{++}]}_{\mathrm{i}}} \tag{80}$$

$$\overline{O}_{\mathrm{TMgMg}} = \frac{11\ \overline{[\mathrm{Mg}^{++}]}_{\mathrm{i}}}{1.11 \cdot 10^{5}\ \overline{[\mathrm{Ca}^{++}]}_{\mathrm{i}} + 11\ \overline{[\mathrm{Mg}^{++}]}_{\mathrm{i}} + 3.663} \tag{81}$$

$$\overline{O}_{\mathrm{TMgC}} = \frac{10^{3}\ \overline{[\mathrm{Ca}^{++}]}_{\mathrm{i}}}{\overline{[\mathrm{Mg}^{++}]}_{\mathrm{i}}}\ \overline{O}_{\mathrm{TMgMg}} \tag{82}$$

$$\overline{O}_{\mathrm{Calse}} = \frac{6}{6 + 5 \Big/ \overline{[\mathrm{Ca}^{++}]}_{\mathrm{i}}} \quad . \tag{83}$$

6.6. Graphical representation of the steady states

Using the formulas given in the previous subsections, the steady states were computed for values of $\overline{V}$ ranging from -90 to 0 mV and $\Phi_{\mathrm{Na,en}} = 0$. A single fixed was found for each value of $\overline{V}$ such that $\overline{V} > -25.6$ mV, and three fixed points otherwise. The accuracy of the results was checked by testing if $\|\mathbf{f}(\overline{\mathbf{x}})\|$ was sufficient small. The stability of the steady states was established using Eq. (11).

For all fixed points, the steady-state transmembrane potential as well as the main intracellular ionic concentrations are displayed in Fig. 7 as a function of the non-specific charge concentration $[\mathrm{NS}]_{\mathrm{i}}$. Five regimes can be observed: there is a single stable fixed point for $[\mathrm{NS}]_{\mathrm{i}} < 37.7$ mM, an unstable fixed point in the interval $37.7 < [\mathrm{NS}]_{\mathrm{i}} < 56$ mM, again a single stable fixed point for $56 < [\mathrm{NS}]_{\mathrm{i}} < 129.5$ mM, one stable and two unstable fixed points for $129.5 < [\mathrm{NS}]_{\mathrm{i}} < 149$ mM, and two stable and one unstable fixed point for $[\mathrm{NS}]_{\mathrm{i}} > 149$ mM. The original initial condition proposed for the Nygren model corresponds to the physiological value $[\mathrm{NS}]_{\mathrm{i}} = 154$ mM and is significantly different from the steady state at the same value of $[\mathrm{NS}]_{\mathrm{i}}$ computed with $\Phi_{\mathrm{Na,en}} = 0$ ($V_m = -74.25$ vs -72.3 mV, $[\mathrm{Na}^{+}]_{\mathrm{i}} = 8.55$ vs 6.39 mM, $[\mathrm{K}^{+}]_{\mathrm{i}} = 129.4$ vs 131.7 mM and $[\mathrm{Ca}^{++}]_{\mathrm{i}} = 0.067$ vs 0.039 μM).

7. Dynamical Regimes in the Nygren model

7.1. System with external stimulation

When a stimulation current is applied, Eq. (B.15) is replaced by Eq. (54), exactly like for the Courtemanche model. In this case, Eq. (28) is not valid anymore and the current $I_{\text{stim}}(t)$ contributes to change the non-specific charge concentration

$$[\text{NS}]_\text{i}(t) = [\text{NS}]_\text{i}(0) - \frac{1}{V_\text{i}F}\left(\Phi_{\text{Na,en}} \cdot t + \int_0^t \text{d}\tau\ I_{\text{stim}}(\tau)\right) \quad . \tag{84}$$

The parameter $\Phi_{\text{Na,en}}$ can be selected so that the second term vanishes. For example, in the Nygren *et al.* paper [3], the value $\Phi_{\text{Na,en}} = -1.68$ pA compensates a train of stimuli with an amplitude of 1.68 nA and a duration of 1 ms delivered at 1 Hz. However, in this paper, we will rather set $\Phi_{\text{Na,en}}$ to zero and consider that the stimulation current acts as a potassium current, so that Eq. (B.17) is replaced by Eq. (56) as in the Courtemanche model. Note that the equation for the cleft potassium concentration remains unchanged. As a consequence, $[\text{NS}]_\text{i}$ is constant for any stimulation protocol.

7.2. Response to large perturbations

A simulation was performed for each of the fixed points, starting from the fixed point as initial condition. After 250 ms of free evolution, a stimulus of amplitude 1 nA was applied for 2 ms. This current was carried by the potassium ions [Eq. (56)], whose concentration $[\text{K}^+]_\text{i}$ was updated at each time step using Eq. (27).

Figure 8 illustrates the 3 regimes observed in the inferior branch of Fig. 7. For $[\text{NS}]_\text{i} < 37.7$ mM, a stable fixed point exists for a high resting potential, but the system is not excitable. In the interval $37.7 < [\text{NS}]_\text{i} < 56$ mM, there exists only an unstable fixed point and the dynamics is auto-oscillatory with a cycle length at steady-state ranging from 580 to 1900 ms (the larger $[\text{NS}]_\text{i}$, the slower the firing rate). For $[\text{NS}]_\text{i} > 56$ mM, the fixed point with the lowest resting potential is stable. A superthreshold stimulation generates an action potential with a duration between 210 and 420 ms measured at 90% repolarization With decreasing values of $[\text{NS}]_\text{i}$, the resting potential becomes elevated and the action potential duration shortens.

Figure 9 illustrates the 3 regimes observed in the superior branch of Fig. 7. The response to stimuli with a duration of 2 ms and an amplitude of $I_{\text{stim}} = \pm 0.1$ nA and ± 1 nA was studied. For $129.5 < [\text{NS}]_{\text{i}} < 149$ mM, the two fixed points of the superior branch are unstable. After the stimulation, the system tends toward the fixed point of the inferior branch. For $[\text{NS}]_{\text{i}} > 149$ mM, there is a stable and an unstable fixed point in the superior branch. When the system starts from the unstable fixed point, it tends toward the stable fixed point of the superior (resp. inferior) branch if the stimulus induces a depolarization (resp. hyperpolarization). When the system starts from the stable fixed point, damped oscillations are observed for low amplitude stimuli (such as 0.1 nA). However, when higher stimulus strengths are used (1 nA) and $[\text{NS}]_{\text{i}} < 197$ mM, the system eventually tends to the stable fixed point of the inferior branch, after a few action potentials are spontaneously generated. In contrast, if $[\text{NS}]_{\text{i}} > 197$ mM, the fixed point is robust against stimulation (at least for $I_{\text{stim}} < 2$ nA). Note that the transmembrane potential reaches its maximum steady-state value in the superior branch at the transition point $[\text{NS}]_{\text{i}} = 197$ mM.

8. Discussion

In this paper, the steady states of atrial cell models were studied, as well as their stability, by determining and analyzing the fixed points of the dynamical system describing the cell kinetics. Analytical tools were used as far as possible in order to compute the comprehensive set of fixed points. In the Fenton–Karma model, a unique stable fixed point was found, which was interpreted as the resting state of the cell. In contrast, the Courtemanche model was shown to have an infinite number of fixed points. These fixed points were classified using a conservation law associated with the capacitor equation relating the transmembrane potential to the ionic concentrations. As a result, at most one of the stable fixed points can be reached, given an initial condition. When no stable fixed point was reachable, simulations showed that the dynamical behavior of the cell is auto-oscillatory. In its original formulation [3], the Nygren model has no fixed point, which means no resting state. Charge conservation was

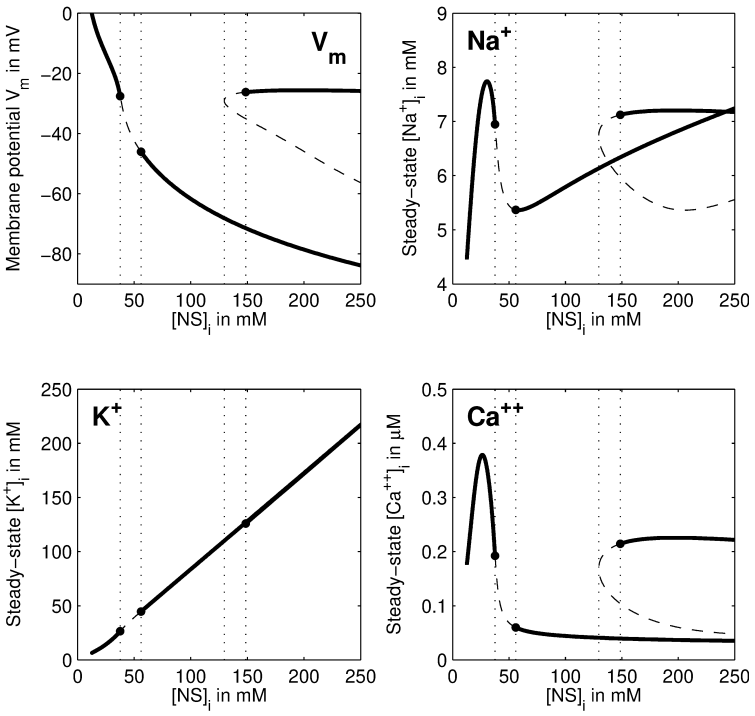

Figure 7: Steady-state transmembrane potential and intracellular ionic concentrations for all fixed points of the Nygren model, represented as a function of the non-specific charge concentration $[NS]_i$. Solid line means stable fixed point and dashed line unstable fixed point. The vertical dotted lines denote the transition between different dynamical regimes.

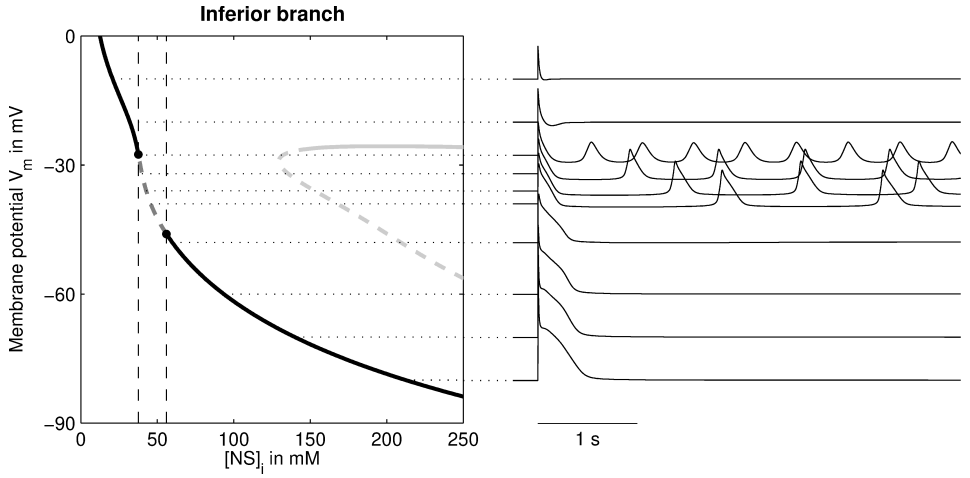

Figure 8: Steady states of the Nygren model. *Left panel*: transmembrane potential of the fixed points belonging to the inferior branch as a function of the non-specific charge concentration $[NS]_i$. The superior branch is shown in light gray. The display correspond to that of Fig. 4. *Right panel*: time course of the transmembrane potential starting from the initial condition indicated by the horizontal dotted line.

restored by setting one of its parameters ($\Phi_{\mathrm{Na,en}}$) to zero. Under this assumption, an infinite number of fixed points and a conservation law were found, resulting in a diagram qualitatively similar to that of the Courtemanche model. However, due to a different formulation of the current I_{K1} [compare Eq. (B.4) with (A.3)], an additional line of fixed points was generated (the superior branch in Fig. 9). As a result, two different stable fixed points are sometimes reachable from one and the same initial condition. The simulations revealed that the fixed point with the lowest transmembrane potential was more robust against the application of impulse stimulation, suggesting that it should be interpreted as the resting state.

The methodology presented here provides a useful guide to a better understanding of the different mathematical models of cell electrophysiology and the impact of their mathematical structure on the resulting dynamical behavior. Although in many of the steady-states the values of some variables are far from physiological conditions (e.g. very low intracellular potassium concentration), the extended view provided by the bifurcation diagram helps

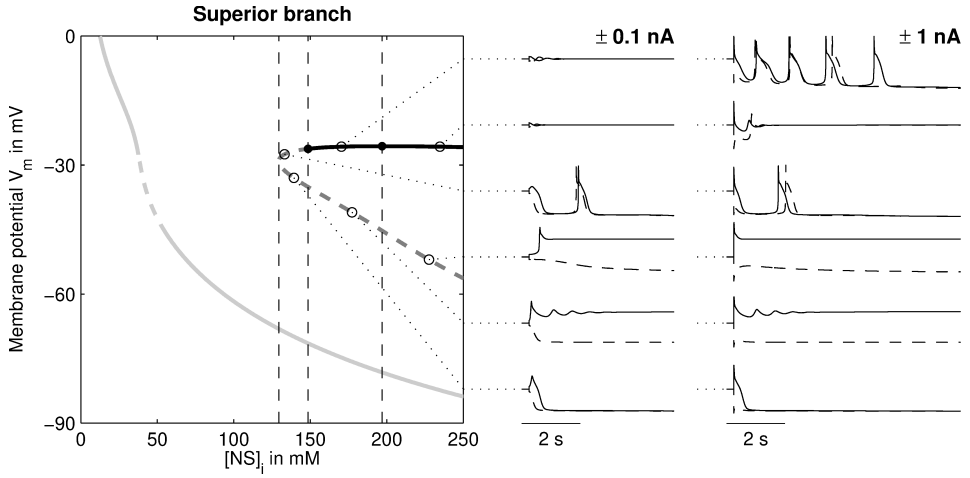

Figure 9: Steady states of the Nygren model. *Left panel*: transmembrane potential of the fixed points belonging to the superior branch as a function of the non-specific charge concentration $[\mathrm{NS}]_\mathrm{i}$. The inferior branch is shown in light gray. The display corresponds to that of Fig. 4. *Right panel*: time course of the transmembrane potential starting from the initial condition indicated by the horizontal dotted line. The stimulus amplitude I_{stim} is 0.1 nA (signals on the left) or 1 nA (signals on the right) with a positive (solid lines) or negative sign (dashed lines)

to visualize and predict the dynamical changes induced by the variation of a parameter of the model studied. After the comprehensive set of steady states has been exhibited, those corresponding to physiological values of $[\mathrm{NS}]_\mathrm{i}$ (typically 150–155 mM) can be extracted for subsequent analysis. For the sake of illustration, the fixed points of the Courtemanche model associated with $[\mathrm{NS}]_\mathrm{i} = 150.2$ mM (physiological value computed from the initial condition, see section 3) are shown in Fig. 10 for decreasing values of the channel conductance g_{K1}. When the original initial condition of the Courtemanche model is used, a reduction of g_{K1} leads to a pacemaker activity. This phenomenon appears on Fig. 10 as a widening of the window of auto-oscillatory dynamics. These plots can be combined to build a bifurcation diagram representing the steady-states and their stability as a function of the control parameter g_{K1} (Fig. 11). This diagram shows that the resting state is unstable for $g_{\mathrm{K1}} < 0.043$ nS/pF when the evolution starts from the original initial condition of the Courtemanche model. Other

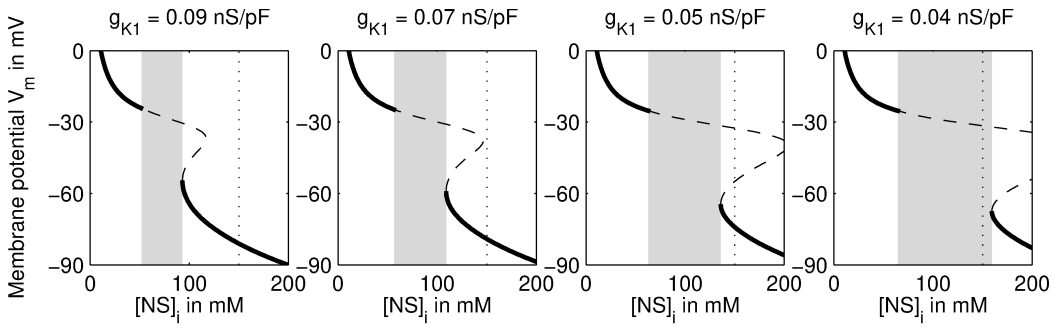

Figure 10: Steady-state transmembrane potential for all fixed points of the Courtemanche model, represented as a function of the non-specific charge concentration $[NS]_i$, like in Fig. 4. From the left to the right panel, the value of the channel conductance g_{K1} is reduced from 0.09 to 0.04 nS/pF. The shaded region indicates an auto-oscillatory dynamics. The vertical dotted line the value of $[NS]_i$ corresponding to the original initial condition of the Courtemanche model.

applications of this methodology include the analysis of the effect of introducing a continuous ionic flux or a leakage current in the cell. This sometimes leads to a pacemaker activity [19].

The approach proposed in this paper is aimed at the exploration of the high-dimensional parameter space of the cell models. Its application may help to identify the conditions leading to spontaneous pacemaker activity.

Acknowledgment

This work was supported by grants from the Theo-Rossi-Di-Montelera Foundation and the Swiss National Sciences Foundation (SNSF). The author wishes to thank Prof. A. van Oosterom for constructive criticism and suggestions on the manuscript.

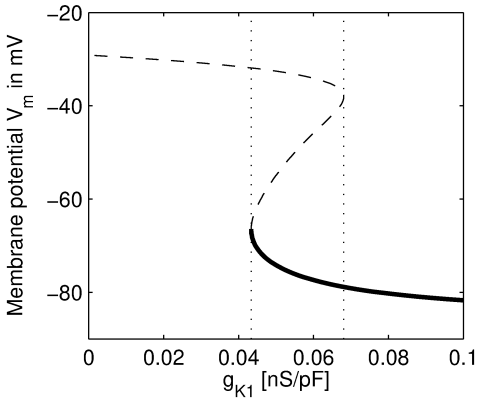

Figure 11: Bifurcation diagram of the Courtemanche model with $[\mathrm{NS}]_\mathrm{i} = 150.2$ mM when g_{K1} is considered as the control parameter. The steady-state potential is represented as a function of g_{K1}. Solid line means stable resting state and dashed line unstable resting state. Bifurcations occur at $g_{\mathrm{K1}} = 0.043$ and 0.068 nS/pF.

Appendix A. The Courtemanche model formulation

Appendix A.1. Ionic currents

The total current of the sodium-, potassium- and calcium-specific ionic channels are formulated by

$$
\begin{aligned}
I_{\mathrm{Na,t}} &= I_{\mathrm{Na}} + I_{\mathrm{b,Na}} = (g_{\mathrm{bNa}} + g_{\mathrm{Na}}\, m^3 hj) \cdot (V - E_{\mathrm{Na}}) && \text{(A.1)}\\
I_{\mathrm{K,t}} &= I_{\mathrm{K1}} + I_{\mathrm{to}} + I_{\mathrm{Kr}} + I_{\mathrm{Kur}} + I_{\mathrm{Ks}} && \text{(A.2)}\\
&= \left(g_{\mathrm{K1}}(V) + g_{\mathrm{to}} o_a^3 o_i + g_{\mathrm{Kr}}(V) x_r + g_{\mathrm{Ks}} x_s^2 + g_{\mathrm{to}} u_a^3 u_i\right) \cdot (V - E_K) && \text{(A.3)}\\
I_{\mathrm{Ca,t}} &= I_{\mathrm{p,Ca}} + I_{\mathrm{CaL}} + I_{\mathrm{b,Ca}} && \text{(A.4)}\\
&= \frac{I_{\mathrm{pCa,max}}}{1 + 5 \cdot 10^{-4} / [\mathrm{Ca}^{++}]_\mathrm{i}} + g_{\mathrm{CaL}} \cdot d \cdot f \cdot f_{\mathrm{Ca}} \cdot (V - 65) + g_{\mathrm{bCa}} \cdot (V - E_{\mathrm{Ca}}) \quad , && \text{(A.5)}
\end{aligned}
$$

where g_{bNa}, g_{Na}, g_{to}, g_{Ks}, g_{to}, g_{CaL}, g_{bCa}, $I_{\mathrm{pCa,max}}$ are positive parameters, and g_{K1} and g_{Kr} are positive functions of V. The Nernst potentials E_{Na} and E_{Ca} are defined by

$$
E_{\mathrm{Na}} = \frac{RT}{F} \log \frac{[\mathrm{Na}^+]_\mathrm{o}}{[\mathrm{Na}^+]_\mathrm{i}} \ , \quad E_{\mathrm{K}} = \frac{RT}{F} \log \frac{[\mathrm{K}^+]_\mathrm{o}}{[\mathrm{K}^+]_\mathrm{i}} \quad \text{and} \quad E_{\mathrm{Ca}} = \frac{RT}{2F} \log \frac{[\mathrm{Ca}^{++}]_\mathrm{o}}{[\mathrm{Ca}^{++}]_\mathrm{i}} \ , \qquad \text{(A.6)}
$$

where R, T and F are the gas constant, the temperature and the Faraday constant, respectively. The index "o" corresponds to extracellular concentrations. In addition, a Na^+/Ca^{2+} ion exchanger current I_{NaCa} and a Na^+–K^+ pump current I_{NaK} are involved:

$$I_{NaCa} = a(V)\cdot[Na^+]_i^3 - b(V)\cdot[Ca^{++}]_i \quad , \tag{A.7}$$

$$I_{NaK} = \frac{I_{NaK,max}(V)}{1+(K_{m,Na}/[Na^+]_i)^{3/2}} \quad , \tag{A.8}$$

where a, b and $I_{NaK,max}$ are positive functions of V. The parameters g_{bNa}, g_{Na}, $K_{m,Na}$, $I_{pCa,max}$, g_{CaL} and g_{bCa} are also positive. The calcium dynamics in the sarcoplasmic reticulum is specified by the currents:

$$I_{up} = \frac{I_{up,max}}{1+K_{up}/[Ca^{++}]_i} \quad , \qquad I_{tr} = \frac{[Ca^{++}]_{up}-[Ca^{++}]_{rel}}{\tau_{tr}} \quad , \tag{A.9}$$

$$I_{rel} = k_{rel}\,u^2 v\,w\,([Ca^{++}]_{rel}-[Ca^{++}]_i) \quad , \qquad I_{leak} = \frac{[Ca^{++}]_{up}}{[Ca^{++}]_{up(max)}}\,I_{up,max} \quad , \tag{A.10}$$

where $I_{up,max}$, K_{up}, τ_{tr}, k_{rel} and $[Ca^{++}]_{up(max)}$ are positive parameters.

Appendix A.2. Evolution equations

The evolution of the system is governed by the following differential equations:

$$C_m\frac{dV}{dt} = -I_{Na,t}-I_{K,t}-I_{Ca,t}-I_{NaCa}-I_{NaK} \tag{A.11}$$

$$\frac{d[Na^+]_i}{dt} = \frac{-3I_{NaK}-3I_{NaCa}-I_{Na,t}}{FV_i} \tag{A.12}$$

$$\frac{d[K^+]_i}{dt} = \frac{2I_{NaK}-I_{K,t}}{FV_i} \tag{A.13}$$

$$B_i\,\frac{d[Ca^{++}]_i}{dt} = \frac{2I_{NaCa}-I_{Ca,t}}{2FV_i} + \frac{V_{up}(I_{leak}-I_{up})+I_{rel}V_{rel}}{V_i} \tag{A.14}$$

$$\frac{d[Ca^{++}]_{up}}{dt} = I_{up}-I_{leak}-I_{tr}\,\frac{V_{rel}}{V_{up}} \tag{A.15}$$

$$B_{rel}\frac{d[Ca^{++}]_{rel}}{dt} = I_{tr}-I_{rel} \quad , \tag{A.16}$$

where V_i, V_{up} and V_{rel} are the volume of the intracellular, uptake and release compartments. In addition, 15 equations of the form of Eq. (4) determine the evolution of the 15 gating variables. The function B_i and B_{rel} are associated with the calcium storage in Troponin (Trpn),

Calmodulin (Cmdn) buffers in the intracellular compartment and Calsequestrin (Csqn) buffers in the release compartment:

$$[\mathrm{Ca}^{++}]_{\mathrm{Trpn}} = \frac{[\mathrm{Trpn}]_{\max}}{1 + K_{\mathrm{m,Trpn}}/[\mathrm{Ca}^{++}]_{\mathrm{i}}}\ , \quad [\mathrm{Ca}^{++}]_{\mathrm{Cmdn}} = \frac{[\mathrm{Cmdn}]_{\max}}{1 + K_{\mathrm{m,Cmdn}}/[\mathrm{Ca}^{++}]_{\mathrm{i}}} \quad \text{(A.17)}$$

$$[\mathrm{Ca}^{++}]_{\mathrm{Csqn}} = \frac{[\mathrm{Csqn}]_{\max}}{1 + K_{\mathrm{m,Csqn}}/[\mathrm{Ca}^{++}]_{\mathrm{rel}}}\ , \quad \text{(A.18)}$$

where $[\mathrm{Buffer}]_{\max}$ and $K_{\mathrm{m,Buffer}}$ are positive constants ("Buffer" stands for Trpn, Cmdn and Csqn). The functions B_{i} and B_{rel} depend on $[\mathrm{Ca}^{++}]_{\mathrm{i}}$ and $[\mathrm{Ca}^{++}]_{\mathrm{rel}}$ respectively, and are defined according to their property:

$$B_{\mathrm{i}}\,\frac{\mathrm{d}[\mathrm{Ca}^{++}]_{\mathrm{i}}}{\mathrm{d}t} = \frac{\mathrm{d}}{\mathrm{d}t}\Big([\mathrm{Ca}^{++}]_{\mathrm{i}} + [\mathrm{Ca}^{++}]_{\mathrm{Trpn}} + [\mathrm{Ca}^{++}]_{\mathrm{Cmdn}}\Big) \quad \text{(A.19)}$$

$$B_{\mathrm{rel}}\,\frac{\mathrm{d}[\mathrm{Ca}^{++}]_{\mathrm{rel}}}{\mathrm{d}t} = \frac{\mathrm{d}}{\mathrm{d}t}\Big([\mathrm{Ca}^{++}]_{\mathrm{rel}} + [\mathrm{Ca}^{++}]_{\mathrm{Csqn}}\Big)\ . \quad \text{(A.20)}$$

Appendix B. The Nygren model formulation

Appendix B.1. Ionic currents

Here, the notations are as far as possible made consistent with those used for the Courtemanche model. The total current of the sodium-, potassium- and calcium-specific ionic channels are

$$I_{\mathrm{Na,t}} = I_{\mathrm{Na}} + I_{\mathrm{b,Na}} \quad \text{(B.1)}$$

$$= g_{\mathrm{Na}}(V)\cdot(0.9\,h_1 + 0.1\,h_2)\left(\mathrm{e}^{FV/RT}[\mathrm{Na}^+]_{\mathrm{i}} - [\mathrm{Na}^+]_{\mathrm{c}}\right) + g_{\mathrm{bNa}}\cdot(V - E_{\mathrm{Na}}) \quad \text{(B.2)}$$

$$I_{\mathrm{K,t}} = I_{\mathrm{K1}} + I_{\mathrm{t}} + I_{\mathrm{sus}} + I_{\mathrm{Kr}} + I_{\mathrm{Ks}} \quad \text{(B.3)}$$

$$= (g_{\mathrm{K1}}(V - E_{\mathrm{K}}) + g_{\mathrm{t}} r\, s + g_{\mathrm{sus}} r_{\mathrm{sus}} s_{\mathrm{sus}} + g_{\mathrm{Kr}}(V) p_a + g_{\mathrm{Ks}} n)\cdot(V - E_K) \quad \text{(B.4)}$$

$$I_{\mathrm{Ca,t}} = I_{\mathrm{p,Ca}} + I_{\mathrm{b,Ca}} \quad \text{(B.5)}$$

$$= \frac{I_{\mathrm{pCa,max}}}{1 + 5\cdot 10^{-4}/[\mathrm{Ca}^{++}]_{\mathrm{i}}} + g_{\mathrm{bCa}}\cdot(V - E_{\mathrm{Ca}}) \quad \text{(B.6)}$$

where g_{bNa}, g_{t}, g_{sus}, g_{Ks}, $I_{\mathrm{pCa,max}}$ and g_{bCa} are positive parameters, and $g_{\mathrm{Na}}(V)$, $g_{\mathrm{K1}}(\cdot)$ and $g_{\mathrm{Kr}}(V)$ are positive functions. The Nernst potentials are computed with respect to the cleft

concentrations:

$$E_{\mathrm{Na}} = \frac{RT}{F}\log\frac{[\mathrm{Na}^+]_\mathrm{c}}{[\mathrm{Na}^+]_\mathrm{i}}\ , \quad E_\mathrm{K} = \frac{RT}{F}\log\frac{[\mathrm{K}^+]_\mathrm{c}}{[\mathrm{K}^+]_\mathrm{i}} \quad \text{and} \quad E_{\mathrm{Ca}} = \frac{RT}{2F}\log\frac{[\mathrm{Ca}^{++}]_\mathrm{c}}{[\mathrm{Ca}^{++}]_\mathrm{i}}\ . \tag{B.7}$$

The calcium current flow in the subsarcolemal space (see Fig. 3) is governed by

$$\begin{aligned} I_{\mathrm{CaL}} &= g_{\mathrm{CaL}}\cdot d_L\cdot\big(f_{\mathrm{Ca}}f_{L_1}+(1-f_{\mathrm{Ca}})f_{L_1}\big)\cdot(V-E_{\mathrm{Ca,app}}) && \text{(B.8)}\\ I_{\mathrm{di}} &= \frac{2FV_\mathrm{d}}{\tau_d}\left([\mathrm{Ca}^{++}]_\mathrm{d}-[\mathrm{Ca}^{++}]_\mathrm{i}\right)\ , && \text{(B.9)} \end{aligned}$$

where g_{CaL}, $E_{\mathrm{Ca,app}}$ and τ_d are positive constants and V_d is the volume of the subsarcolemal space. The $\mathrm{Na}^+/\mathrm{Ca}^{2+}$ ion exchanger current I_{NaCa} and the Na^+–K^+ pump current I_{NaK} are formulated as:

$$\begin{aligned} I_{\mathrm{NaK}} &= I_{\mathrm{NaK,max}}\cdot\frac{[\mathrm{K}^+]_\mathrm{c}}{[\mathrm{K}^+]_\mathrm{c}+k_{\mathrm{NaK,K}}}\cdot\frac{[\mathrm{Na}^+]_\mathrm{i}^{3/2}}{[\mathrm{Na}^+]_\mathrm{i}^{3/2}+k_{\mathrm{NaK,Na}}^{3/2}}\cdot\frac{V+150}{V+200} && \text{(B.10)}\\ I_{\mathrm{NaCa}} &= k_{\mathrm{NaCa}}\,\frac{[\mathrm{Na}^+]_\mathrm{i}^3\,[\mathrm{Ca}^{++}]_\mathrm{c}\,\mathrm{e}^{\gamma VF/RT}-[\mathrm{Na}^+]_\mathrm{c}^3\,[\mathrm{Ca}^{++}]_\mathrm{i}\,\mathrm{e}^{(1-\gamma)VF/RT}}{1+d_{\mathrm{NaCa}}\left([\mathrm{Na}^+]_\mathrm{c}^3\,[\mathrm{Ca}^{++}]_\mathrm{i}+[\mathrm{Na}^+]_\mathrm{i}^3\,[\mathrm{Ca}^{++}]_\mathrm{c}\right)}\ , && \text{(B.11)} \end{aligned}$$

where $I_{\mathrm{NaK,max}}$, $k_{\mathrm{NaK,K}}$, $k_{\mathrm{NaK,Na}}$, k_{NaCa}, γ, and d_{NaCa} are positive parameters. The calcium dynamics in the sarcoplasmic reticulum is described by the following currents (see Fig. 3):

$$\begin{aligned} I_{\mathrm{up}} &= I_{\mathrm{up,max}}\,\frac{[\mathrm{Ca}^{++}]_\mathrm{i}/k_{\mathrm{cyca}}-k_{\mathrm{xcs}}^2[\mathrm{Ca}^{++}]_{\mathrm{up}}/k_{\mathrm{srca}}}{([\mathrm{Ca}^{++}]_\mathrm{i}+k_{\mathrm{cyca}})/k_{\mathrm{cyca}}+k_{\mathrm{xcs}}([\mathrm{Ca}^{++}]_{\mathrm{up}}+k_{\mathrm{srca}})/k_{\mathrm{srca}}} && \text{(B.12)}\\ I_{\mathrm{tr}} &= \frac{2FV_{\mathrm{rel}}}{\tau_{\mathrm{tr}}}\big([\mathrm{Ca}^{++}]_{\mathrm{up}}-[\mathrm{Ca}^{++}]_{\mathrm{rel}}\big) && \text{(B.13)}\\ I_{\mathrm{rel}} &= \alpha_{\mathrm{rel}}\left(\frac{F_2}{F_2+1/4}\right)^2\left([\mathrm{Ca}^{++}]_{\mathrm{rel}}-[\mathrm{Ca}^{++}]_\mathrm{i}\right)\ , && \text{(B.14)} \end{aligned}$$

where $I_{\mathrm{up,max}}$, k_{cyca}, k_{xcs}, k_{srca}, τ_{tr} and α_{rel} are positive parameters, V_{rel} is the volume of the release compartment and F_2 is a gating variable.

Appendix B.2. Evolution equations

The evolution equations for the transmembrane potential and for the ionic concentrations (including the calcium buffers) read:

$$C_m \frac{\mathrm{d}V}{\mathrm{d}t} = -I_{\mathrm{Na,t}} - I_{\mathrm{K,t}} - I_{\mathrm{Ca,t}} - I_{\mathrm{CaL}} - I_{\mathrm{NaCa}} - I_{\mathrm{NaK}} \tag{B.15}$$

$$\frac{\mathrm{d}[\mathrm{Na}^+]_\mathrm{i}}{\mathrm{d}t} = \frac{-3I_{\mathrm{NaK}} - 3I_{\mathrm{NaCa}} - I_{\mathrm{Na,t}} - \Phi_{\mathrm{Na,en}}}{FV_\mathrm{i}} \tag{B.16}$$

$$\frac{\mathrm{d}[\mathrm{K}^+]_\mathrm{i}}{\mathrm{d}t} = \frac{2I_{\mathrm{NaK}} - I_{\mathrm{K,t}}}{FV_\mathrm{i}} \tag{B.17}$$

$$\frac{\mathrm{d}[\mathrm{Ca}^{++}]_\mathrm{i}}{\mathrm{d}t} = \frac{2I_{\mathrm{NaCa}} + I_{\mathrm{di}} - I_{\mathrm{Ca,t}} + I_{\mathrm{rel}} - I_{\mathrm{up}}}{2FV_\mathrm{i}} - \frac{\mathrm{d}O}{\mathrm{d}t} \tag{B.18}$$

$$\frac{\mathrm{d}[\mathrm{Ca}^{++}]_\mathrm{d}}{\mathrm{d}t} = \frac{-I_{\mathrm{di}} - I_{\mathrm{CaL}}}{2FV_\mathrm{d}} \tag{B.19}$$

$$\frac{\mathrm{d}[\mathrm{Ca}^{++}]_{\mathrm{up}}}{\mathrm{d}t} = \frac{I_{\mathrm{up}} - I_{\mathrm{tr}}}{2FV_{\mathrm{up}}} \tag{B.20}$$

$$\frac{\mathrm{d}[\mathrm{Ca}^{++}]_{\mathrm{rel}}}{\mathrm{d}t} = \frac{I_{\mathrm{tr}} - I_{\mathrm{rel}}}{2FV_{\mathrm{rel}}} - \frac{\mathrm{d}O_{\mathrm{Calse}}}{\mathrm{d}t} \tag{B.21}$$

$$\frac{\mathrm{d}[\mathrm{Na}^+]_\mathrm{c}}{\mathrm{d}t} = \frac{[\mathrm{Na}^+]_\mathrm{b} - [\mathrm{Na}^+]_\mathrm{c}}{\tau_{\mathrm{Na}}} + \frac{3I_{\mathrm{NaK}} + 3I_{\mathrm{NaCa}} + I_{\mathrm{Na,t}} + \Phi_{\mathrm{Na,en}}}{FV_\mathrm{c}} \tag{B.22}$$

$$\frac{\mathrm{d}[\mathrm{K}^+]_\mathrm{c}}{\mathrm{d}t} = \frac{[\mathrm{K}^+]_\mathrm{b} - [\mathrm{K}^+]_\mathrm{c}}{\tau_{\mathrm{K}}} + \frac{-2I_{\mathrm{NaK}} + I_{\mathrm{K,t}}}{FV_\mathrm{c}} \tag{B.23}$$

$$\frac{\mathrm{d}[\mathrm{Ca}^{++}]_\mathrm{c}}{\mathrm{d}t} = \frac{[\mathrm{Ca}^{++}]_\mathrm{b} - [\mathrm{Ca}^{++}]_\mathrm{c}}{\tau_{\mathrm{Ca}}} + \frac{I_{\mathrm{CaL}} + I_{\mathrm{Ca,t}} - 2I_{\mathrm{NaCa}}}{2FV_\mathrm{c}} \tag{B.24}$$

$$\frac{\mathrm{d}O_\mathrm{C}}{\mathrm{d}t} = 2 \cdot 10^5 \, [\mathrm{Ca}^{++}]_\mathrm{i} \, (1 - O_\mathrm{C}) - 476 \, O_\mathrm{C} \tag{B.25}$$

$$\frac{\mathrm{d}O_{\mathrm{TC}}}{\mathrm{d}t} = 7.84 \cdot 10^4 \, [\mathrm{Ca}^{++}]_\mathrm{i} \, (1 - O_{\mathrm{TC}}) - 392 \, O_{\mathrm{TC}} \tag{B.26}$$

$$\frac{\mathrm{d}O_{\mathrm{TMgC}}}{\mathrm{d}t} = 2 \cdot 10^5 \, [\mathrm{Ca}^{++}]_\mathrm{i} \, (1 - O_{\mathrm{TMgC}} - O_{\mathrm{TMgMg}}) - 6.6 \, O_{\mathrm{TMgC}} \tag{B.27}$$

$$\frac{\mathrm{d}O_{\mathrm{TMgMg}}}{\mathrm{d}t} = 2 \cdot 10^3 \, [\mathrm{Mg}^{++}]_\mathrm{i} \, (1 - O_{\mathrm{TMgC}} - O_{\mathrm{TMgMg}}) - 666 \, O_{\mathrm{TMgMg}} \tag{B.28}$$

$$\frac{\mathrm{d}O_{\mathrm{Calse}}}{\mathrm{d}t} = 480 \, [\mathrm{Ca}^{++}]_{\mathrm{rel}} \, (1 - O_{\mathrm{Calse}}) - 400 \, O_{\mathrm{Calse}} \tag{B.29}$$

where V_i, V_d, V_c, V_{up}, V_{rel} are the volume of the compartments, $\Phi_{\mathrm{Na,en}}$ is a constant, the index "b" denotes (constant) bulk concentrations, the intracellular magnesium concentration

$[Mg^{++}]_i$ is a constant, and O is defined as

$$O = 0.08\ O_{TC} + 0.16\ O_{TMgC} + 0.045\ O_C \quad . \tag{B.30}$$

In addition, 12 equations of the form of Eq. (4) determine the evolution of the gating variables. m, h_1, h_2, d_L, f_{L_1}, f_{L_2}, r, s, r_{sus}, s_{sus}, n, p_a. The gating variables F_1 and F_2 are coupled and are governed by the equations:

$$\frac{dF_1}{dt} = r_{recov}(1 - F_1 - F_2) - r_{act}F_1 \tag{B.31}$$

$$\frac{dF_2}{dt} = r_{act}F_1 - r_{inact}F_2 \quad , \tag{B.32}$$

where r_{recov}, r_{act} and r_{inact} are positive functions of $[Ca^{++}]_i$ and $[Ca^{++}]_d$.

References

[1] R. Plonsey, R. C. Barr, Bioelectricity: A Quantitative Approach, 2nd Edition, Kluwer Academic Plenum Publishers, 2000.

[2] M. Courtemanche, R. J. Ramirez, S. Nattel, Ionic mechanisms underlying human atrial action potential properties: Insights from a mathematical model, Am. J. Physiol. 275 (1998) H301–H321.

[3] A. Nygren, C. Fiset, L. Firek, J. W. Clark, D. S. Lindblad, R. B. Clark, W. R. Giles, Mathematical model of an adult human atrial cell: the role of K^+ currents in repolarization, Circ. Res. 82 (1998) 63–81.

[4] D. Attwell, I. Cohen, D. Eisner, Membrane potential and ion concentration stability conditions for a cell with a restricted extracellular space., Proc R Soc Lond B Biol Sci 206 (1979) 145–61.

[5] S. Genet, R. Costalat, J. Burger, The influence of plasma membrane electrostatic properties on the stability of cell ionic composition., Biophys J 81 (2001) 2442–57.

[6] S. Guan, Q. Lu, K. Huang, A discussion about the DiFrancesco–Noble model, J. Theor. Biol. 189 (1997) 27–32.

[7] A. R. Yehia, D. Jeandupeux, F. Alonso, M. R. Guevara, Hysteresis and bistability in the direct transition from 1:1 to 2:1 rhythm in periodically driven single ventricular cells., Chaos 9 (1999) 916–931.

[8] T. J. Hund, J. P. Kucera, N. F. Otani, Y. Rudy, Ionic charge conservation and long-term steady state in the Luo–Rudy dynamic cell model, Biophys. J. 81 (2001) 3324–31.

[9] J. Kneller, R. J. Ramirez, D. Chartier, M. Courtemanche, S. Nattel, Time-dependent transients in an ionically based mathematical model of the canine atrial action potential, Am. J. Physiol. Heart Circ. Physiol. 282 (2002) H1437–51.

[10] M. Courtemanche, R. J. Ramirez, S. Nattel, Ionic targets for drug therapy and atrial fibrillation-induced electrical remodeling: Insights from a mathematical model., Cardiovasc Res 42 (1999) 477–89.

[11] Z. Syed, E. Vigmond, S. Nattel, L. J. Leon, Atrial cell action potential parameter fitting using genetic algorithms, Med. Biol. Eng. Comput. 43 (2005) 561–71.

[12] A. M. Goodman, R. A. Oliver, C. S. Henriquez, P. D. Wolf, A membrane model of electrically remodelled atrial myocardium derived from in vivo measurements., Europace 7 Suppl 2 (2005) 135–45.

[13] J. R. Ehrlich, T.-J. Cha, L. Zhang, D. Chartier, P. Melnyk, S. H. Hohnloser, S. Nattel, Cellular electrophysiology of canine pulmonary vein cardiomyocytes: action potential and ionic current properties, J. Physiol. 551 (2003) 801–13.

[14] A. Varghese, G. R. Sell, A conservation principle and its effect on the formulation of Na-Ca exchanger current in cardiac cells., J Theor Biol 189 (1997) 33–40.

[15] F. Fenton, A. Karma, Vortex dynamics in three-dimensional continuous myocardium with fiber rotation: Filament instability and fibrillation, Chaos 8 (1) (1998) 20–47.

[16] R. M. Corless, G. H. Gonnet, D. E. G. Hare, D. J. Jeffrey, D. E. Knuth, On the Lambert W function, Adv Comput Math 5 (1996) 329–59.

[17] L. P. Endresen, K. Hall, J. S. Hoye, J. Myrheim, A theory for the membrane potential of living cells, Eur Biophys J 29 (2000) 90–103.

[18] C. Zemlin, Rhythms and wave propagation in the heart, Ph.D. thesis, Humboldt-Universität, Berlin, Germany (2002).

[19] V. Jacquemet, Pacemaker activity resulting from the coupling with nonexcitable cells, Phys Rev E 74 (1) (2006) 011908.